Research Article

Yunpeng Hu, Zhuorui Zhang, Zhiwei Yan, Yucang Dong, Yongquan Zhu*, Zhenrong Xia, Zhenwei Yan, Tongda Guo, and Wanxue Long

Discrete element simulation study on effects of grain preferred orientation on micro-cracking and macro-mechanical behavior of crystalline rocks

https://doi.org/10.1515/rams-2024-0001 received October 21, 2023; accepted February 29, 2024

Abstract: Grain-preferred orientation significantly influences the brittle fracture mechanism and failure mode of crystalline rocks. However, current grain-based models (GBMs) based on particle flow code (PFC) software are mostly proposed on the basis of the Voronoi tessellation method for grain boundary generation, which is difficult to simulate the heterogeneity of microstructure such as shape and orientation of rock minerals. To study the effect of grain-preferred orientation on macroscopic mechanical properties and microscopic characteristics of crystalline rocks, a novel grain-based microstructure transformation

method (MTM) is proposed. Based on the MTM, a GBM with a target aspect ratio and crystal orientation is obtained by transforming the Voronoi crystal geometry through a planar coordinate mapping. Specifically, embedded FISH language is used to control random mineral seed size and distribution pattern to generate Tyson polygons. A polygon geometry that satisfies the rock texture is obtained as a grain boundary by spatially transforming the vertex of the Tyson polygon. The transformed complex geometry is taken as the crystal structure of the GBM, and the Lac du Bonnet granite models with different aspect ratios and crystal orientations were developed in PFC^{2D}. Finally, a series of unconfined compressive strength tests are performed in PFC^{2D} to verify the proposed modeling methods for the geometric variation of the crystals and to study the effects of the preferred orientation of the grains on the macroscopic mechanical properties and microscopic fracture mechanisms of the crystalline rocks from different perspectives.

Keywords: microscopic rupture mechanisms, discrete element method, grain-based model, aspect ratio, grain-preferred orientation

* Corresponding author: Yongquan Zhu, State Key Laboratory of Mechanical Behavior and System Safety of Traffic Engineering Structures, Shijiazhuang Tiedao University, Shijiazhuang, 050043, China, e-mail: yongquanzhu_2022@163.com

Yunpeng Hu: State Key Laboratory of Geohazard Prevention and Geoenvironment Protection, Chengdu University of Technology, Chengdu, 610059, China; China Railway No. 5 Engineering Group Co. Ltd, Guiyang, China

Zhuorui Zhang: State Key Laboratory of Geohazard Prevention and Geoenvironment Protection, Chengdu University of Technology, Chengdu, 610059, China

Zhiwei Yan: College of Water Resource and Hydropower, Sichuan University, Sichuan 610065, China

Yucang Dong: Hebei Technology Innovation Center for Intelligent Development and Control of Underground Built Environment, School of Urban and Geology Engineering, Hebei GEO University, Shijiazhuang, 050030, China; State Key Laboratory of Mechanical Behavior and System Safety of Traffic Engineering Structures, Shijiazhuang Tiedao University, Shijiazhuang, 050043, China

Zhenrong Xia, Zhenwei Yan: China Railway No. 5 Engineering Group Co. Ltd, Guiyang, China

Tongda Guo: Guiyang Urban Rail Transit Group Co. Ltd, Guiyang Guizhou, 550081, China

Wanxue Long: Guizhou Transportation Planning Survey & Design Academe Co. Ltd, Guiyang, 550001, China

1 Introduction

Natural rocks are heterogeneous bodies that are composed of a variety of minerals. The properties of the rock are generally determined by the type of mineral, compositional content, mineral size, and arrangement within the rock [1,2]. Under external loading, this heterogeneity leads to large differences in mechanical properties including strength and deformation of homogeneous rocks with similar mineral content [3,4]. As studies delve deeper into smaller scales, it has become evident that local stress concentration at the scale of rock mineral crystals

fundamentally causes macroscopic rock damage [5,6]. The presence of discontinuous surface defects significantly influences the mechanical properties and stability of the rock mass. Moreover, crystal orientation and intergrowth patterns are crucial in determining the anisotropic behavior of rocks, which influence their response to stress, shear, and deformation [7,8]. Therefore, the effect of microgeometry on rock strength and deformation needs to be studied at the grain scale to further investigate the intrinsic mechanisms of rock damage.

In the past few decades, scholars have conducted numerous experimental studies on non-homogeneous rocks. exploring the impact of microstructural heterogeneity on macroscopic mechanical properties [9,10]. Research findings indicated a complex nonlinear relationship between the macroscopic mechanical properties of rocks and various fine mineral parameters [11-13]. An increase in plagioclase feldspar mineral content corresponded to increased uniaxial compressive strength of the rock, while the rock's cracking stress was significantly influenced by mineral composition, showing a positive correlation [14,15]. The average size of mineral crystals significantly influences the uniaxial compressive strength of rocks, particularly when the grain size is less than 1 mm [16]. Microscopic experiments highlighted that the grain arrangement significantly impacts rock properties, leading to stress concentration and the emergence of local cracks, ultimately affecting the damage pattern of the rock [17]. In summary, crystal properties and spatial geometric distribution of minerals significantly influence strength-related mechanical parameters of rocks, such as modulus of elasticity, uniaxial compressive strength, and splitting tensile strength [18,19]. Nonetheless, precise control of these factors in actual experiments posed challenges due to the wide dispersion of properties in naturally obtained specimens and the influence of the test operator's subjectivity. Conducting systematic studies of inhomogeneous rocks at the fine mineral scale using experimental methods still posed significant challenges in understanding physical and mechanical properties.

The advancement in numerical simulation software has enabled a detailed exploration of the damage mechanisms within fractured rock masses [20,21]. In order to accurately simulate and observe the destruction process of rocks, the grain-based model (GBM) approach has received increasing attention from researchers [5,22,23]. It was an effective method that could simulate crystalline rocks and observe the rock destruction process from multiple scales [24,25]. GBM implementation in universal distinct element code (UDEC), 3 dimension distinct element code (3DEC), and particle flow code (PFC) has facilitated the investigation of microscopic fracture and micromechanical behavior of

rock [26,27]. Intergranular deformation and fracture between blocks were simulated by assigning a Coulomb sliding model, representing particles as block cells. The simulation, while dividing the internal block into multiple zones to simulate intracrystalline deformation, is limited in explicitly simulating intracrystalline cracking due to restricted damage between particles [28,29]. The damage process of rocks with crystallographic orientation had been studied using 3DEC, but it was also limited to the effect of crystallographic orientation on macroscopic mechanical properties. The results of the study do not go deeper into the microscopic level involving the intracrystalline damage situation [30]. However, the influence of crystal properties on the characterization of crystalline rocks was still focused on by some schoolers, and they finally made some technical breakthroughs through in-depth research. Some scholars present a numerical approach that assesses the influence of mineral heterogeneity and rock mass defects (pore structures) on the fracturing performance of Soundless Cracking Demolition Agents at the grain size level by 3DEC. Moreover, intergranular and intracrystalline fracturing of the assembly was also simulated by utilizing a dual-layer discretization technique [31].

In PFC-GBMs, rocks were viewed as an aggregate of balls. These balls were divided into different groups according to the shape of the crystals in the crystalline rocks and assigned different material properties [32]. The intracrystalline and intergranular damage in crystalline rocks were characterized by the failure of the bonded particle model, including the parallel bonded model (PBM), smooth jointed model (SJM), and flat joint model (FJM). They enabled realistic simulation of intracrystalline and intergranular damage in crystalline rocks. However, PBM has some limitations in the simulation process due to its inability to resist bending moments in grain contacts. The direct tensile strength of the model would be too large when matched to the unconfined compressive strength of a typical dense rock. The FIM proposed by Potyondy [33–36] can solve this problem. The most significant advantage of the FJM is that it successfully modeled the sustained rotational resistance after bond breakage between rock particles. The contact model provides a finite size, linear elasticity, and macroscopic behavior of bonded or frictional interfaces that may withstand partial damage, allowing to simulate the microstructure of angularly interlocked particles. Additionally, SJM simulated the mechanical behavior between intergroup crystals. A novel particle model (nGBM) introduced in the two-dimensional PFC 5.0 aimed to simulate the microcracking process in crystalline brittle rock [37] explores the critical impact of rock cracking on geological applications, focusing on the influence of mechanical parameters at the rock grain scale on fluid-driven cracking behavior. Numerical

simulations employing the GBM approach in the discrete element method (DEM) indicate increased simulated rock strength with larger grain size [38]. The research team investigated the influence of brittleness on the microcracking behavior of crystalline rock through GBM implemented in a two-dimensional PFC [39]. These findings emphasize the role of mineral strength and bonding in characterizing rock brittleness at a microscale.

Previous research results obtained through experiments and numerical simulation all demonstrated that the microstructure of crystalline rocks had a large influence on the macroscopic strength and microscopic fracture process of rocks, including the size and morphology of minerals, spatial distribution, and alignment direction [40-42]. The microscopic crack evolution of rocks that penetrate deeply into the crystal interior under loading can be observed by PFC-GBMs. However, conventional PFC-GBMs still have certain shortcomings. As shown in Figure 1, it was well known that recrystallized quartz minerals in granites had an obviously preferred orientation $(\theta)^{\circ}$) in some cases. However, the existing GBMs in PFC-GBMs failed to control both the size distribution and the preferred orientation of the mineral grain. Initially, some scholars proposed a method to construct GBMs in PFC^{2D} based on the standard Tyson polygon generation procedure and the PBM-SIM contact model, which provided an idea for studying rock mineral crystals in PFC [38,43]. Subsequently, the FJM-SJM contact model began to be gradually accepted and widely used in the simulation studies of mineral crystals in order to make the contacts between crystals more consistent with reality [37]. Prior research via experiments and numerical simulations consistently showed that the microstructure of crystalline rocks significantly impacts both the macroscopic strength and microscopic fracture process, encompassing mineral size, morphology, spatial distribution, and alignment direction [40-42]. PFC-GBMs enable the observation of microscopic crack evolution deeply within the crystal interior of rocks under loading. Nevertheless, conventional

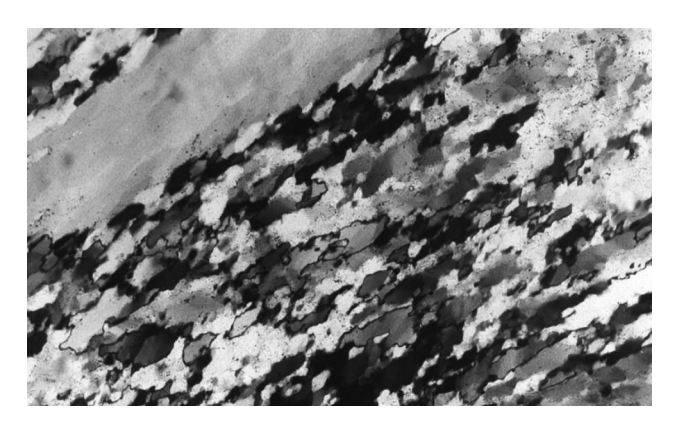


Figure 1: Microstructure of quartz-oriented distribution in granite [47].

PFC-GBMs exhibit specific limitations. In certain cases, recrystallized quartz minerals in granites exhibited a clearly defined preferred orientation, as depicted in Figure 1. However, the current GBMs within PFC-GBMs inadequately address both mineral grain size distribution and preferred orientation. Initially, scholars suggested a method to develop GBMs in PFC^{2D} using the standard Tyson polygon generation procedure and the PBM-SIM contact model, offering a framework to investigate rock mineral crystals in PFC [38,43]. Later, the FJM-SJM contact model gained acceptance and extensive usage in simulation studies of mineral crystals to improve contact consistency between crystals and reality [37]. Currently, research efforts in algorithmic enhancements predominantly emphasize crystal size distribution, with relatively fewer investigations addressing changes in grain shape structure. The impact of crystal morphology on rock properties has been insufficiently investigated. Advancements in this technique allowed for crystal morphology characterization through digital image processing methods and the integration of discrete fracture meshes into the GBM using statistical techniques [44]. However, this progress largely pertained to rocks with relatively regular crystallization processes, neglecting crystalline rocks with significant aspect ratios and pronounced tendencies like those shown in Figure 1. Consequently, this approach, reliant on mathematical statistics, fails to accurately represent the meritocratic orientation of real crystal distributions and the apparent morphology of aspect ratios, resulting in simulation outcomes discrepant from reality [45,46].

However, it can be found by summarizing the results of previous studies that the existing GBMs in PFC-GBMs failed to control both the size distribution and the preferred orientation of mineral grains, leading to the inability to observe the evolution of microscopic cracks of rocks that penetrate deeply into the crystal interior under loading condition. To realize the simulation of grain-preferred orientation in PFC^{2D}, it is necessary to first develop modeling techniques that can build rock grains with certain aspect ratios. In this research, we proposed a novel GBM that can generate a certain aspect ratio and preferred orientation of grain by the microstructure transformation method (MTM) to study the effect of the angle (/°) between the direction of the principal stress of a crystalline rock under load and the grain orientation on rock fracture process. A standardized calibration process for the PFC-GBMs model parameters was also provided. Based on the new model proposed in this article, the relationship among grain preferred orientation, macroscopic strength, microscopic fracture evolution, and damage mode of rock was studied. The rest of this article is organized as follows: Section 2 presents the algorithm for generating specimens with a certain aspect ratio and

crystallization angle in PFC-GBMs. The idea of numerical experiments and the whole process for microparameters calibration involved in the proposed PFC-GBM is introduced in Section 3. In Section 4, the influence of the preferred orientation of the grain on the mechanical properties of the rock by conducting a series of numerical experiments was investigated. Finally, a conclusion of the study is provided in Section 5. The novelty of the research results in this article is mainly in two aspects. One is that a novel generation procedure of GBMs that can generate a specified aspect ratio and crystallographic orientation was proposed in PFC^{2D}, and the other is the effects of grain-preferred orientation on macroscopic mechanical properties and microscopic rupture mechanisms of crystalline rock materials were investigated from multiple scales.

2 Numerical approach

2.1 FJM and SJM in PFC

According to the documentation of PFC, PFC^{2D} software simulates a realistic deformed body through many rigid non-deformable discs and the contact behavior between discs and discs [33]. Generally, PBM and FJM can be used to simulate cemented materials like rocks. The FJM has a better characterization of the mechanical behavior of the rock, although the computational complexity is higher. The FJM model discretizes the contact surface between particles into several cells (see Figure 2 from the PFC manual), each of which can undergo damage. The force ($F^{(e)}$) and bending moment ($M^{(e)}$) are applied at the center of each

cell, and the mechanical update of the contact surface is calculated as the sum of the cells on the contact surface

$$\begin{cases}
\mathbf{F}^{(e)} = F_n^{(e)} \widehat{\mathbf{n}}_{\mathbf{c}} + \mathbf{F}_{\mathbf{s}}^{(e)} \\
\mathbf{M}^{(e)} = M_t^{(e)} \widehat{\mathbf{n}}_{\mathbf{c}} + \mathbf{M}_{\mathbf{b}}^{(e)}
\end{cases} (1)$$

where $F_n^{(e)}$ is the normal stress of unit, $F_s^{(e)}$ is the shear stress of unit, and $M_t^{(e)}$ and $M_b^{(e)}$ are twisting moment and bending moment of unit, respectively. In the two-dimensional model, $M_t^{(e)}$ is equal to 0.

The SJM is used to simulate the mechanical behavior between two planes (Figure 3). The parallel bonding of adjacent particles through which the joint passes is replaced by the SJM. The SJM is typically used to avoid the unwanted mechanical dilation and additional frictional resistance that can be observed during particle interlocking/sliding over neighboring particles. The SJM in PFC provides two types of nodal interfaces: bonded interface and unbonded

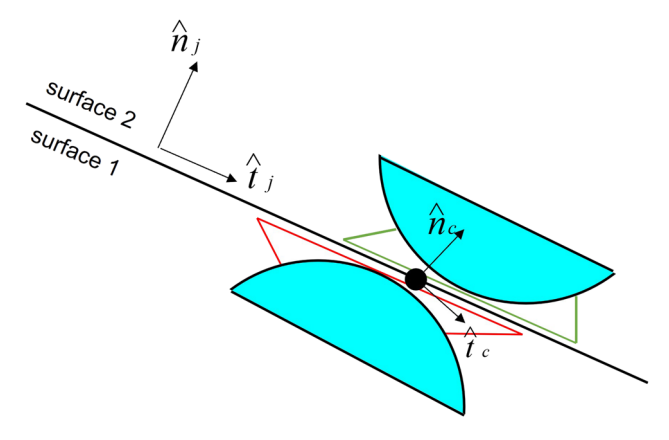


Figure 3: Smooth-joint contact in PFC^{2D}.

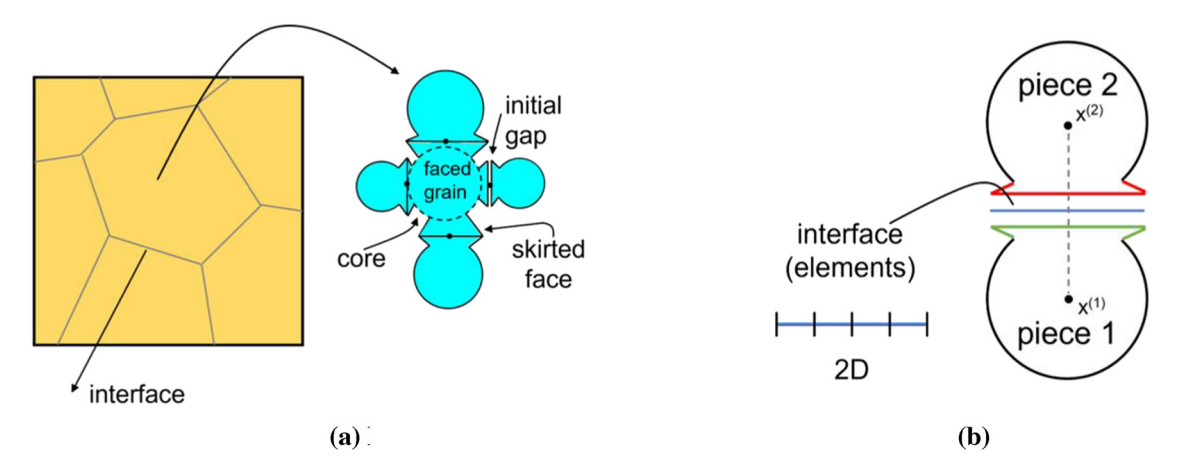


Figure 2: Schematic diagram of the FJM model in PFC^{2D}: (a) flat-jointed material and (b) flat-joint contact.

interface. The mechanical behavior of the bonded interface is linear-elastic. The bond fracture occurs when the contact force exceeds the ultimate strength. The unbonded interface comes with an expansive frictional slip between them. It adjusts the shear force at the joint surface by the Coulomb limit, and the joint surface does not rotate.

2.2 GBMs

The development of the GBM aimed to overcome the limitations associated with inadequate inclusion when simulating rock-like materials in PFC. The GBM elevates the compression—tension ratio of rock materials to a realistic level, offering a more precise depiction of the mechanical behavior of crystalline rocks. In PFC-GBMs, the linear parallel bond model (LPBM) primarily simulates the mechanical behavior of individual minerals, whereas the SJM interfaces between grains. Based on research findings highlighting limitations in characterizing the tensile strength ratio and strength envelope of rocks, the FJM was introduced to simulate mineral mechanical behavior. Despite being more computationally intensive than the LPBM, the FJM provides superior accuracy

in representing the mechanical behavior of intact rock-like materials [48].

In general, the shape of grains is simulated by Tyson polygons. It is found that Tyson polygons can simulate the actual mineral shape well, and the GBM generated by this grain structure can accurately reflect the mechanical properties of hard rock (*i.e.*, granite). A Tyson polygon is a set of continuous polygons consisting of perpendicular bisectors connecting line segments of two neighboring points. Each vertex of it is the center of the outer circle of each triangle. Many instances in nature have the shape of Tyson polygons, for example, leaf veins, dragonfly wings, giraffe body texture, land cracks, including the crystalline shape of rocks. The process of generating Tyson polygons can be done in the following steps (Figure 4):

- 1) Scattering seeds uniformly in space. Tyson polygons with a certain distribution of sizes can be generated by controlling the distance between seeds.
- 2) Constructing a Delaunay triangle mesh from the discrete point data and recording the triangle numbers and the corresponding vertex information.
- 3) Connecting the outer circle of the Delaunay triangle network. This is done by drawing the perpendiculars of each triangle edge. These mid-pipelines form the

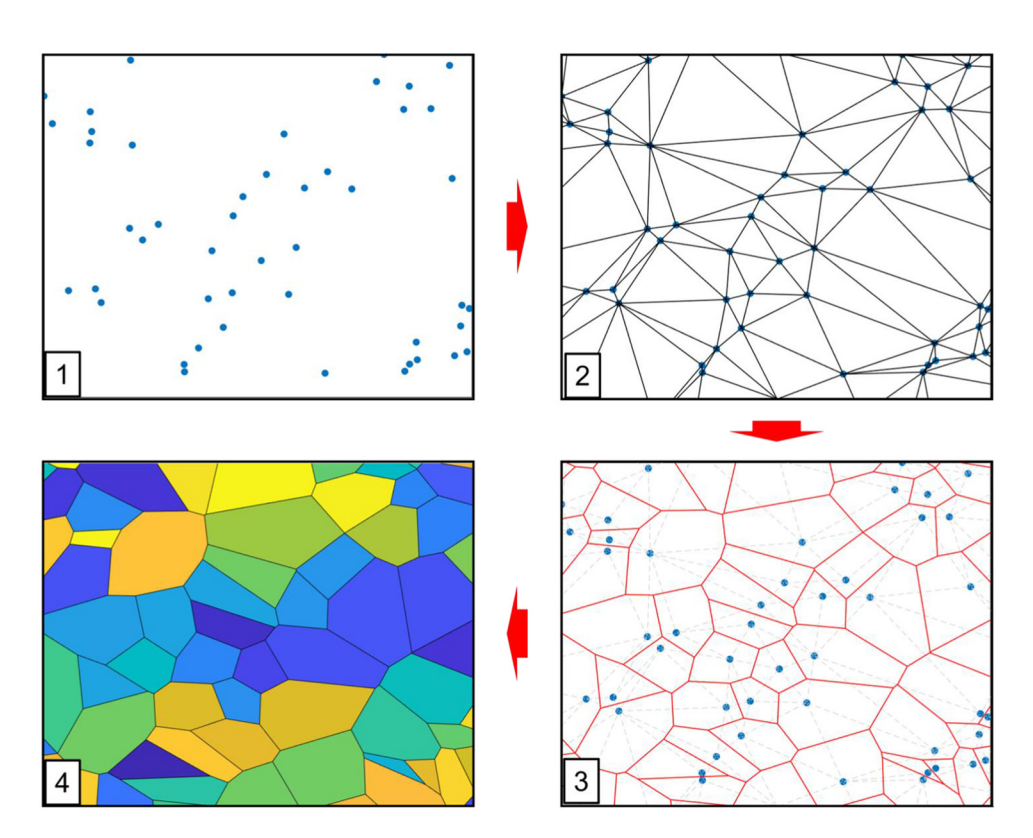


Figure 4: The generation process of normal Tyson polygons.

sides of the Tyson polygon, and the intersection of the mid-pipelines is the vertex of the corresponding Tyson polygon.

 Connecting the corresponding vertices to form a Tyson polygon according to spatial relationship.

The mineral boundaries are generated by the above Tyson polygon program (named Voronoi tessellation method [VTM], in PFC) and imported into the PFC, and the GBM is generated by giving the particles different groupings and set contacts between balls. In general, the contacts in the GBM can be categorized into intragranular and intergranular contacts. Different microscopic parameters are used for different groups of contacts, which increases the heterogeneity of the rock mass and allows a better simulation of various mechanical properties of the rock. In early GBM studies [23,49], for GBMs with n minerals, the parameters of the n minerals are usually calibrated independently, and the contact between different minerals is assigned the same mechanical parameters. In all, there are a total of (n + 1) contact types in the final PFC model. However, many studies [37] have shown that this simulation method does not represent well the inhomogeneity of the rock. Subsequent studies focused on the inhomogeneity of the intergranular contacts of various types of minerals. Different contact parameters were used for the contacts between different crystals. Consequently, a total of (n + $(n + 1) \times n/2$) contact types were obtained in the final model. This type of numerical model is more responsive to the mechanical properties of the rock [45].

2.3 Directional GBM generation procedure in PFC^{2D}

The conventional Tyson polygon generation process in PFC (*i.e.*, VTM) is mainly to assign different groups to the PFC particles according to their geometrical properties after generation and then assign the corresponding contact model and contact parameters.

In this article, the morphology and growth direction of crystals are further considered. After the generation of VTM, the standard Tyson polygons are secondary generated into Tyson-like polygons with a certain aspect ratio and a certain growth direction. Consequently, the intact specific generation process is as follows (Figure 5):

 First, N groups (N is a count of mineral type) of ball particles are generated in PFC using the FISH language. The average size of each group of ball particles is equal to the average size of that mineral type (to increase heterogeneity, the ball size can be set to a positive-terrestrial distribution). The proportion of particle volume of each mineral to the volume of all ball particles is the same as that of the real rock minerals. After the model is statically balanced, the circle centers of these ball particles are used as seeds for generating traditional Tyson polygons. These seeds are used to generate standard Tyson polygons according to the procedure in Section 2.2 (Figure 5a). The generated Voronoi shapes are representative of the mineral composition of the original rock. The generated Tyson polygon topology is stored in an external.txt file.

- 2) The Voronoi topology information in step 1 is scaled according to the target aspect ratio, as shown in Figure 5(b). It is worth noting that it should be ensured that the number of PFC particles contained in a single Voronoi remains the same before and after scaling, and the area of Voronoi should remain the same before and after scaling. If we take the *y*-axis as the long-axis direction, the *x*-axis as the short-axis direction, and the target aspect ratio as *R*, then multiply all the vertex *x*-coordinate values in the file by $\sqrt{\frac{1}{R}}$, and the *y*-axis coordinate values by \sqrt{R} .
- 3) The vertex information in step 2 is rotated in plane space according to the following equation and rotated to the target loading angle, as shown in Figure 5(c). Then, the vertex information of the secondary processing is saved.

$$\begin{cases} x' = \cos(\varphi) \cdot x - \sin(\varphi) \cdot y \\ y' = \sin(\varphi) \cdot x + \cos(\varphi) \cdot y' \end{cases}$$
 (2)

where v(x, y) is the Tyson polygon vertex position after the aspect ratio scaling in step 2; v'(x', y') is the new vertex position after the spatial rotation; and φ is the target loading angle.

4) The model particles are generated in PFC^{2D} according to the appropriate porosity as well as size. Afterward, the

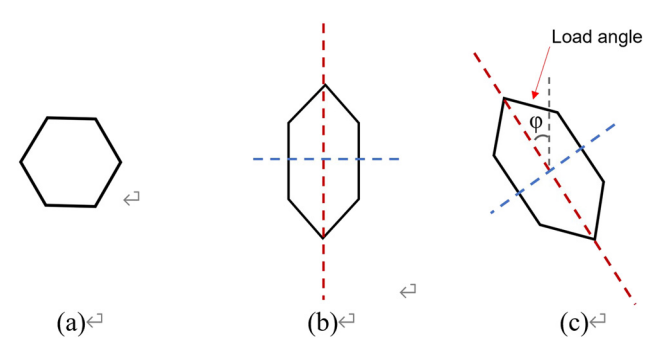


Figure 5: Preferred orientation distributions of Voronoi tessellations generated by the MTM.

particles are grouped according to the geometric information in step 3 to form the GBM geometry model, and the excess particles are removed to form the target-size specimen. The entire particle generation process is shown in Figure 6.

3 Numerical setup

3.1 GBM calibration

This study focuses on simulating Lac Du Bonnet (LDB) granite, a type of crystalline rock. The rock comprises the following mineral percentages: alkali feldspar (48%), plagioclase (17%), quartz (29%), and mica (primarily biotite, constituting 6%). Mineral grain seed diameters are as follows: alkali feldspar (3-4 mm), plagioclase (2-6 mm), quartz (2-3 mm), and biotite (2 mm). As described in Section 2.1, the simulation utilized the FJM and SJM models for intra- and intergranular contact simulation (Figure 7). PFC's minimum particle radius is 0.15 mm, with a maximum-to-minimum particle radius ratio of $R_{\text{max}}/R_{\text{min}} = 1.66$ [45]. The calibration process involves both intracrystalline and intergranular parameter adjustments. Initially, individual minerals underwent calibration (intracrystalline parameter calibration), followed by adjusting the intergranular contact parameters for the entire specimen.

The calibration of microscale parameters in PFC significantly differs from deriving common macroscale mechanical parameters like Young's modulus (E), Poisson ratio (ν), unconfined compressive strength (UCS) (σ_c), and tensile strength (σ_t) directly from physical tests. This discrepancy

underscores the critical nature of calibrating microscale parameters for accurate simulations. Calibration in PFC is a meticulous process that often involves iterative trials informed by physical test results. Fortunately, established principles and empirical procedures aid this calibration process, serving as a guide for determining these microscale parameters. In this study, specific fine view parameters were employed and are detailed in Table 1.

The contact parameters are mainly divided into deformation parameters (Young's model, Poisson ratio) and strength parameters (cohesion, friction angle, tension). Before the calibration of individual mineral parameters, the deformation parameters are first calibrated. The target elastic modulus and Poisson ratio are matched by adjusting the parameters of fi emod and fi kratio. After the calibration of deformation parameters, the contact strength parameters are then adjusted. In general, the tensile strength of the specimen is more influenced by the parameter of fj_ten, and higher tensile strength is obtained by increasing the value of fi_ten. The final compressive strength is generally influenced by the parameters of fi coh and fi fa, but fj fa mainly affects the triaxial test results and has little effect on uniaxial test results. In the process of calibrating strength parameters, the deformation parameters also need to be fine-tuned.

The intergranular parameters are selected as the average of the mineral parameters on both sides and multiplied by an attenuation factor. The intergranular parameters are influenced by five attenuation coefficients, namely, α_E , α_k , α_t , α α _coh, and α _fa, which characterize the deformation and strength changes of the specimens. α E and α k affect the modulus of elasticity and Poisson's ratio of the specimen, respectively. While α _ten, α _coh, and α fa affect the tensile strength and compressive strength of the specimen. The

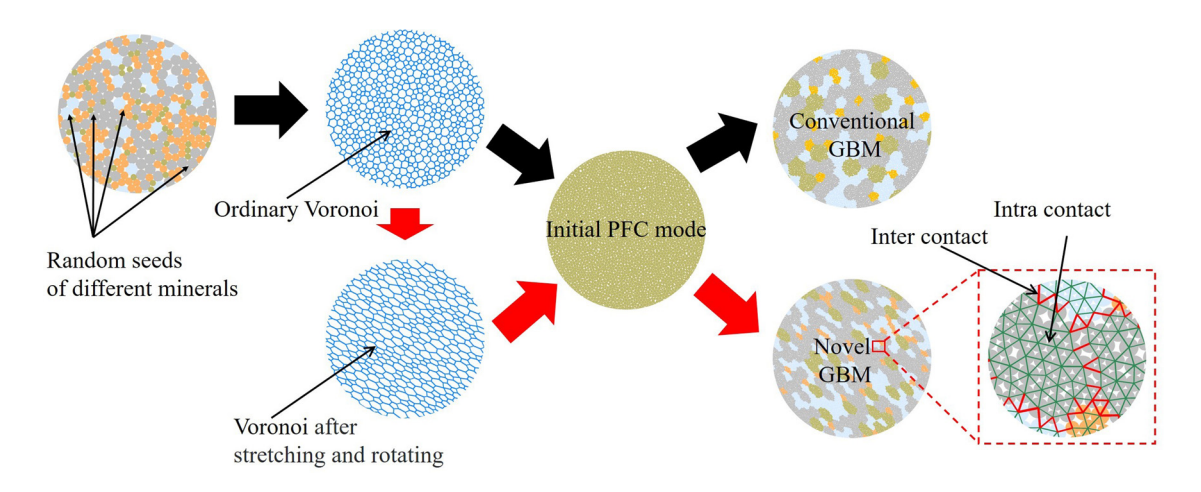


Figure 6: Generation procedure of GBM.

8 — Yunpeng Hu et al. DE GRUYTER

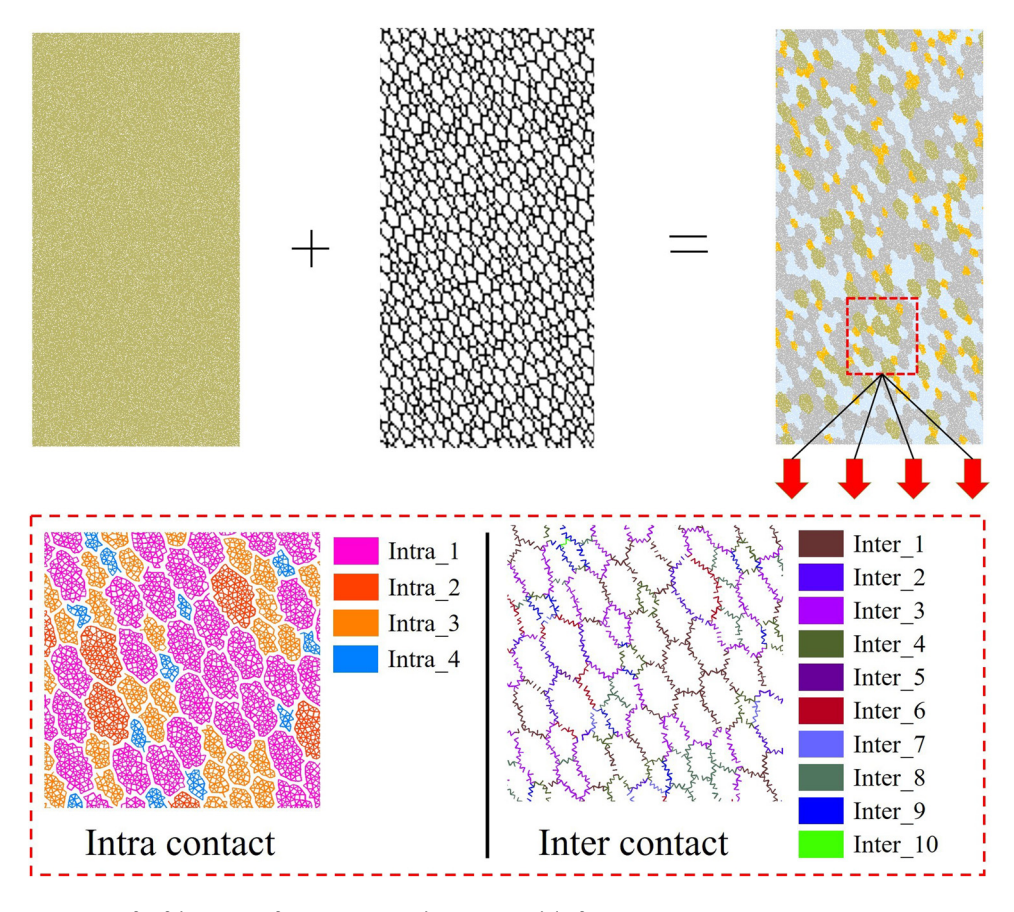


Figure 7: Generation process for fabrication of LDB granite and contact model of GBM.

Table 1: Main macroscopic and microscopic mechanical parameters of model

fj_emod - effective modulus of FJM α_fa - attenuation friction angle fj_kratio - normal-to-shear stiffness ratio of FJM $\varphi_{\rm b}$ – friction angle fj_ten - tensile strength of FJM u – friction coefficient fj_coh - cohesion of FJM $N_{\rm r}$ – number of elements in radial direction $c_{\rm b}$ – cohesion fj_fa - friction angle of FJM α_E – attenuation effective modulus K_n/K_s – normal-to-shear stiffness ratio α_k – attenuation normal-to-shear stiffness ratio D - particle size α _coh – attenuation cohesion ρ – particle density α_ten - attenuation tensile strength E_c – effective modulus

calibration process is shown in Figure 8. After the calibration process according to the previous method, the final calibration results and the actual LDB granite test parameters are shown in Table 2. The microscopic contact parameters are shown in Table 3.

3.2 Numerical simulations

The present study focuses on the comparison of UCS test results and does not involve triaxial loading (Figure 9). The

peak stress, Young's module, Poisson ratio, and tensile strength of the specimens were calibrated by uniaxial compressive tests and Brazilian tests during the numerical simulation. The uniaxial compressive test is performed by applying pressure at a fixed rate in opposite directions through the wall at the top and bottom ends. The axial strain is the ratio of the change in distance between the walls at both ends to the initial distance during the simulation. The tensile strength of the rock was calibrated using the Brazilian test. The upper and lower walls apply only relative vertical velocities to squeeze the specimen, and all

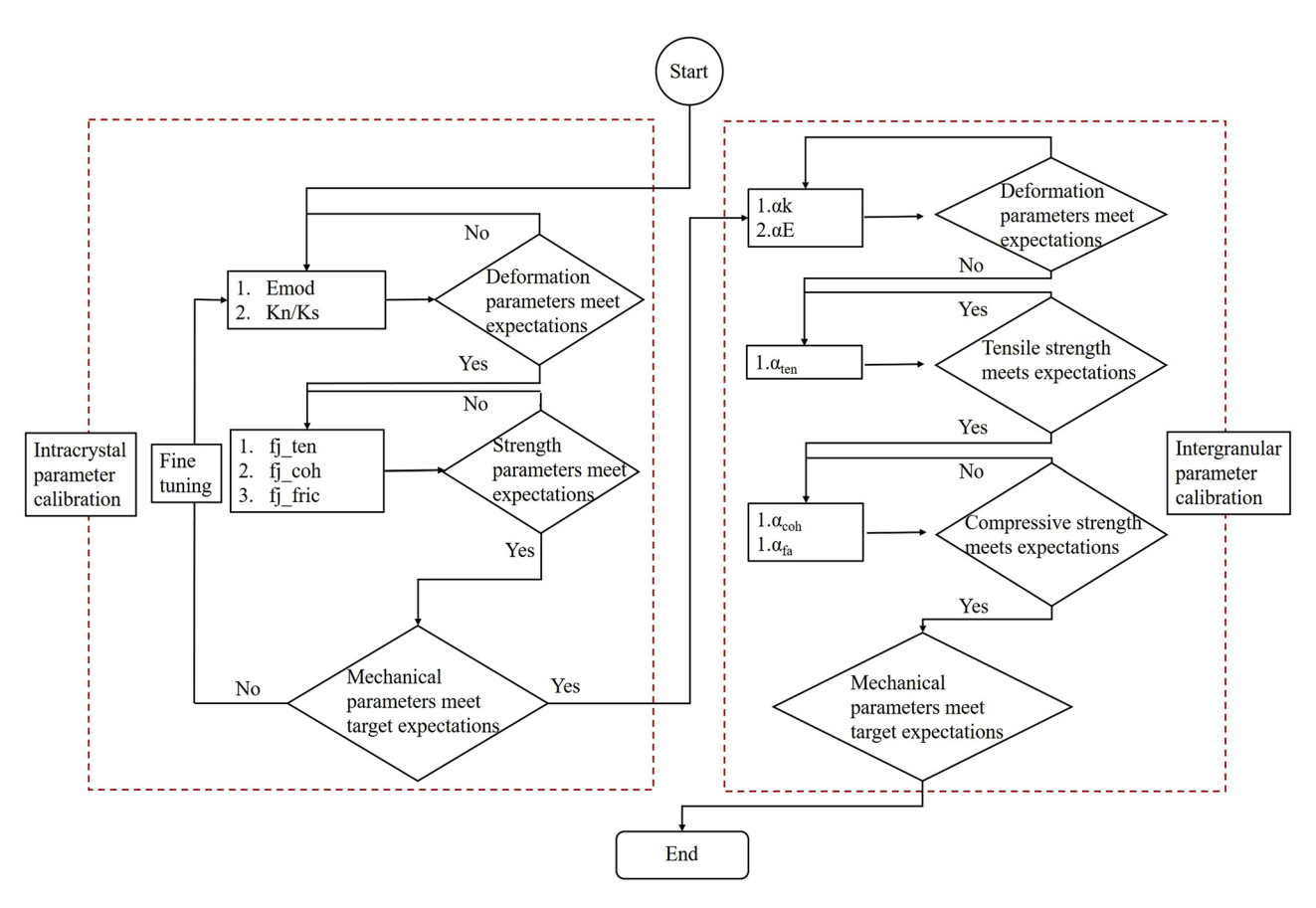


Figure 8: Calibration process based on SJM and FJM.

Table 2: Macro-mechanical properties of LdB granite [5]

| Macro-mechanical properties | Experiment | Simulation |
|---|-----------------|------------|
| Young's modulus, E (GPa) | 69 ± 5.8 | 69.84 |
| Poisson ratio, v | 0.26 ± 0.04 | 0.25 |
| Uniaxial compressive strength, σ_c (MPa) | 200 ± 22 | 199.08 |
| Tensile strength, $\sigma_{\rm t}$ (MPa) | 7.4 ± 1.04 | 7.43 |

contact forces applied on the wall are monitored and summed during the calculation. The tensile strength was calculated by the following equation:

$$\sigma_{\rm t} = \frac{2P}{\pi Dt},\tag{3}$$

where P is the average value of the reaction force on the wall at the upper and lower ends of the disc, D is the diameter of the disc specimen, and t is the thickness of the disc (t=1 in two-dimensional analysis). The rock simulation models with different aspect ratios and preferred orientations were established according to the MTM proposed in Chapter 2 (Figure 10). The macroscopic mechanical strength and microscopic fracture evolution of the specimens were

investigated for different aspect ratios (1.25, 1.50, 1.75, 2.00) and crystal orientations (0°, 30°, 45°, 60°, 90°).

Table 3: Microscopic properties of four minerals and their grain boundaries

| Microscale parameters | Alkali feldspar | Plagioclase | Quartz | Biotite | |
|---------------------------|---|-------------|--------|---------|--|
| | Microscale parameters of intracrystalline group | | | | |
| D_{\min} | 0.15 | 0.15 | 0.15 | 0.15 | |
| $D_{\rm max}/D_{\rm min}$ | 1.66 | 1.66 | 1.66 | 1.66 | |
| $ ho$ (kg·m $^{-3}$) | 2,650 | 2,650 | 2,650 | 2,650 | |
| $E_{\rm c}$ (GPa) | 53 | 70 | 73 | 100 | |
| $K_{\rm n}/K_{\rm s}$ | 1.5 | 1.5 | 1.5 | 1.5 | |
| u | 0.5 | 0.5 | 0.5 | 0.5 | |
| $N_{\rm r}$ | 4 | 4 | 4 | 4 | |
| c_{b} | 235 | 290 | 475 | 220 | |
| $arphi_{ m b}$ | 10 | 13 | 2 | 10 | |
| | Microscale parameters of intergranular group | | | | |
| a_ <i>E</i> | 0.65 | _ | _ | _ | |
| $a_{\underline{k}}$ | 2.5 | _ | _ | _ | |
| a_{-coh} | 0.35 | _ | _ | _ | |
| $a_{ m ten}$ | 0.32 | _ | _ | _ | |
| a_ _{fa} | 1.0 | _ | _ | _ | |

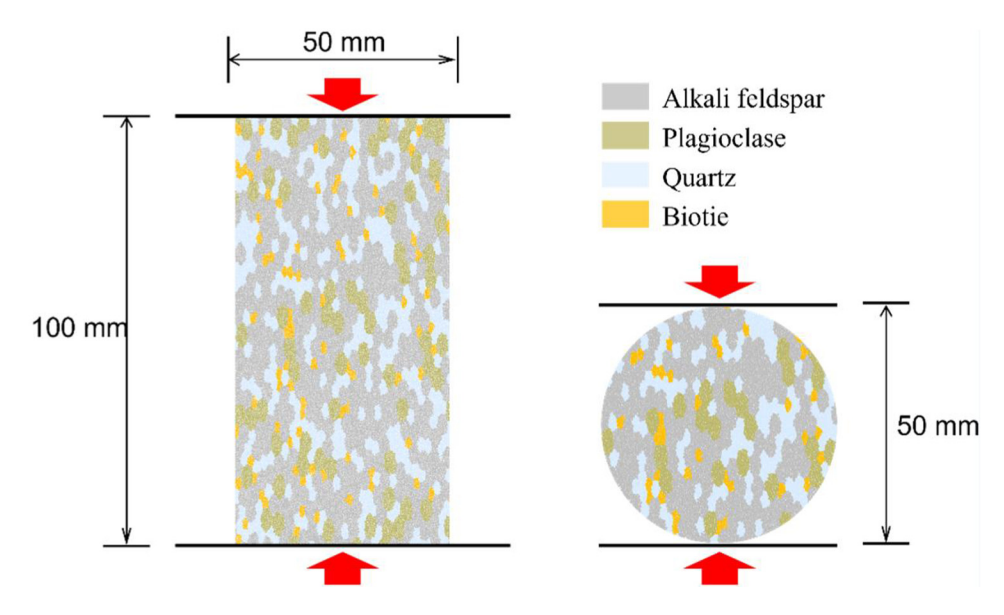


Figure 9: Physical geometric parameters and loading conditions of the numerical model.

4 Numerical results

In this section, numerical simulation experiments of the corresponding model were carried out based on the new modeling approach. The effects of the aspect ratio of rock grain and distribution of rock grain preferred orientations (θ) on stress–strain response, fracture characteristics, failure mode under uniaxial compression tests were mainly analyzed. Actually, θ was that the long axis of the grain was biased in a certain direction in space. Similar to the state of the geotechnical forces in practical engineering, there was also a certain angle λ between the principal stress direction and the crystal orientation. However, as the numerical experiments in this article were carried out in a vertical loading mode, the two directions were parallel, then, λ was also equal to 0. When $\theta = 90^{\circ}$, the preferred orientation was perpendicular to the direction of axial compression. At this point both θ and λ were equal to 90°.

4.1 Stress-strain response

The stress-strain curves obtained from the uniaxial compression test for specimens, illustrated in Figure 11 (taking an aspect ratio of 2.0 as an example), reveal a consistent pattern. These curves display an initial rapid ascent to the peak, followed by a subsequent decline in stress as the axial strain increases. Notably, variations in rock grain orientation influence the strain at which the specimens

reach their peak strength. In Figure 12a, the trends in UCS with respect to the angle θ showcase a distinctive pattern of decrease and subsequent increase with the increment in θ . Notably, larger aspect ratios correspond to lower minimum UCS values. Furthermore, when the rock grain's aspect ratio is small (e.g., R = 1.25 and 1.50), the curve demonstrates a gradual incline, contrasting sharply with a steeper slope observed at larger aspect ratios (e.g., R =1.75 and 2.00), culminating in a peak at a 90° orientation. At this juncture, the UCS experiences an increase ranging from 11 to 70% compared to the scenario where R = 1.25. Figure 12b illustrates the UCS variation concerning the aspect ratio for different orientation models. Observations indicate that when θ is below 30°, the UCS tends to exhibit a slow decline with increasing aspect ratio. Conversely, when θ surpasses 60°, the UCS tends to rise in conjunction with the aspect ratio.

In general, the UCS of the specimens with different aspect ratios had similar trends with the change of preferred orientation (Figure 13). However, the inflection point of the UCS curve seemed to occur at around 30°. Since only two characteristic angles of grain orientation in the range of 0 to 30° were selected to study, several additional numerical simulations were carried out for orientations of 5°, 10°, 15°, 20°, and 25°. In order to exclude the influence of the aspect ratio on the experimental results, three additional conditions with aspect ratios of 1.25, 1.50, and 1.75 were also considered in the analytical discussion of the model. The final numerical experimental results are shown in Figure 14. It can be seen that there is an inflection point in

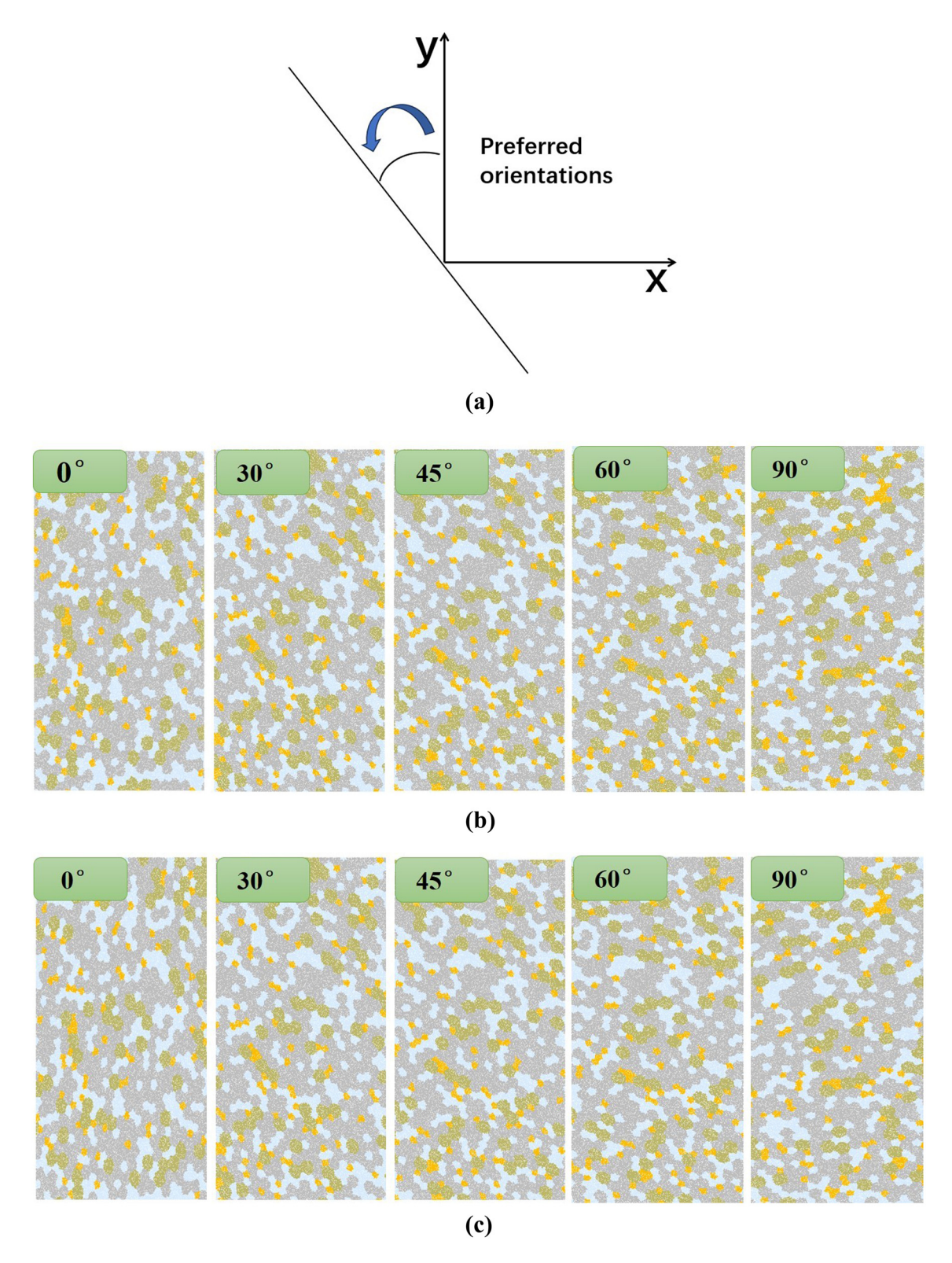


Figure 10: Numerical models of rocks with different aspect ratios and preferred orientations. (a) Schematic of preferred orientation angle, (b) aspect ratio = 1.25, (c) aspect ratio = 1.50, (d) aspect ratio = 1.75, and (e) aspect ratio = 2.00.

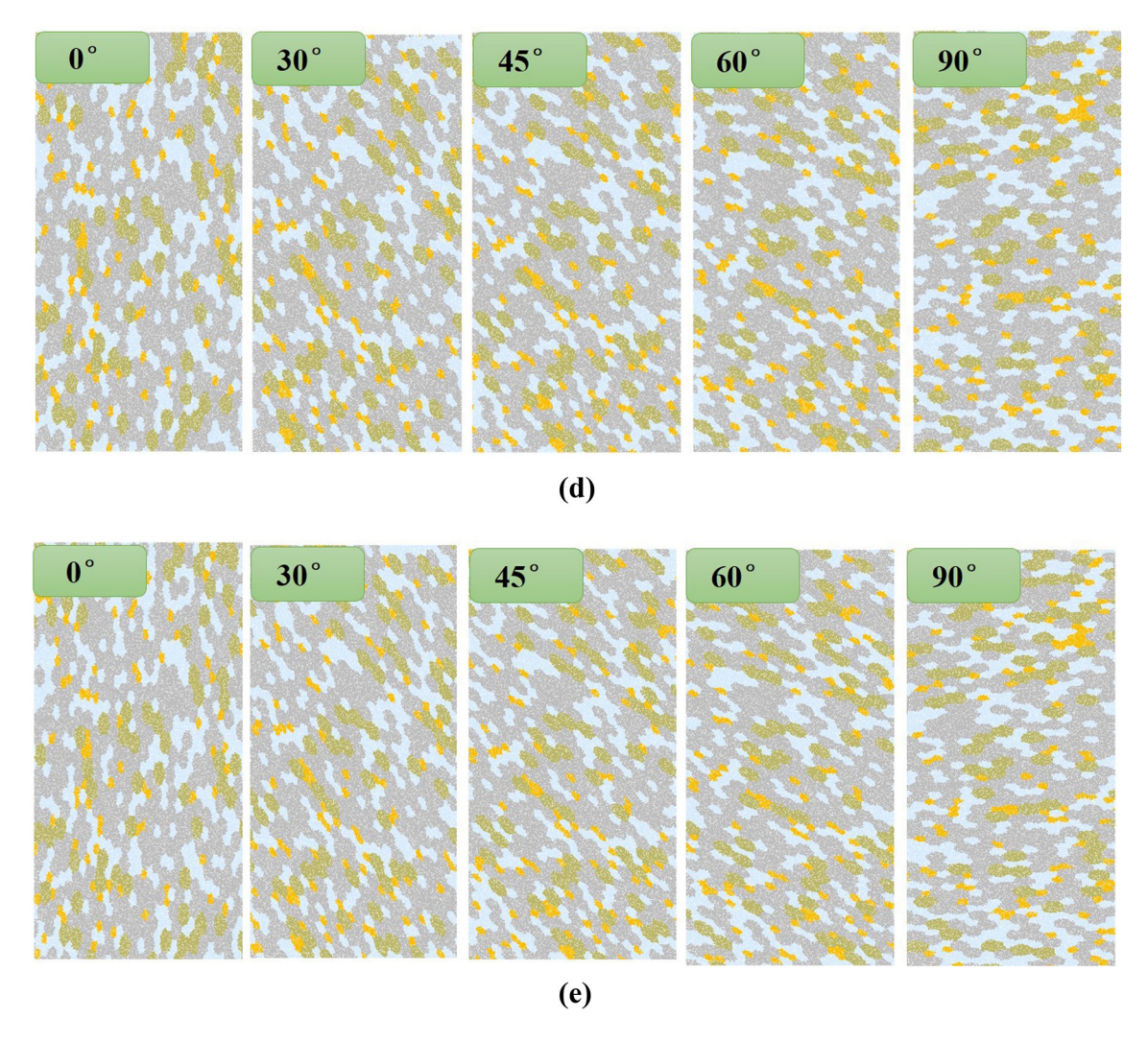


Figure 10: (Continued)

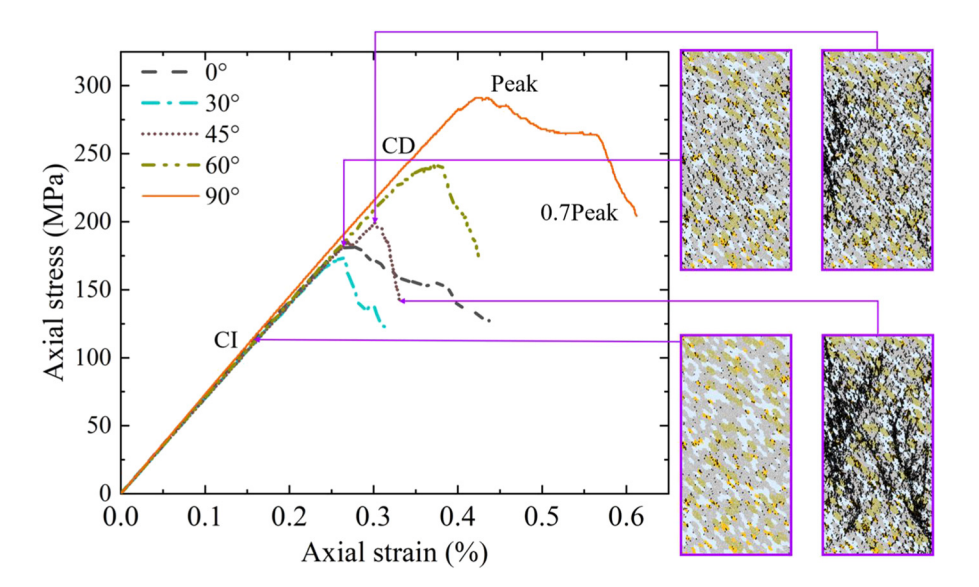


Figure 11: Stress–strain curve of the specimen under uniaxial compression.

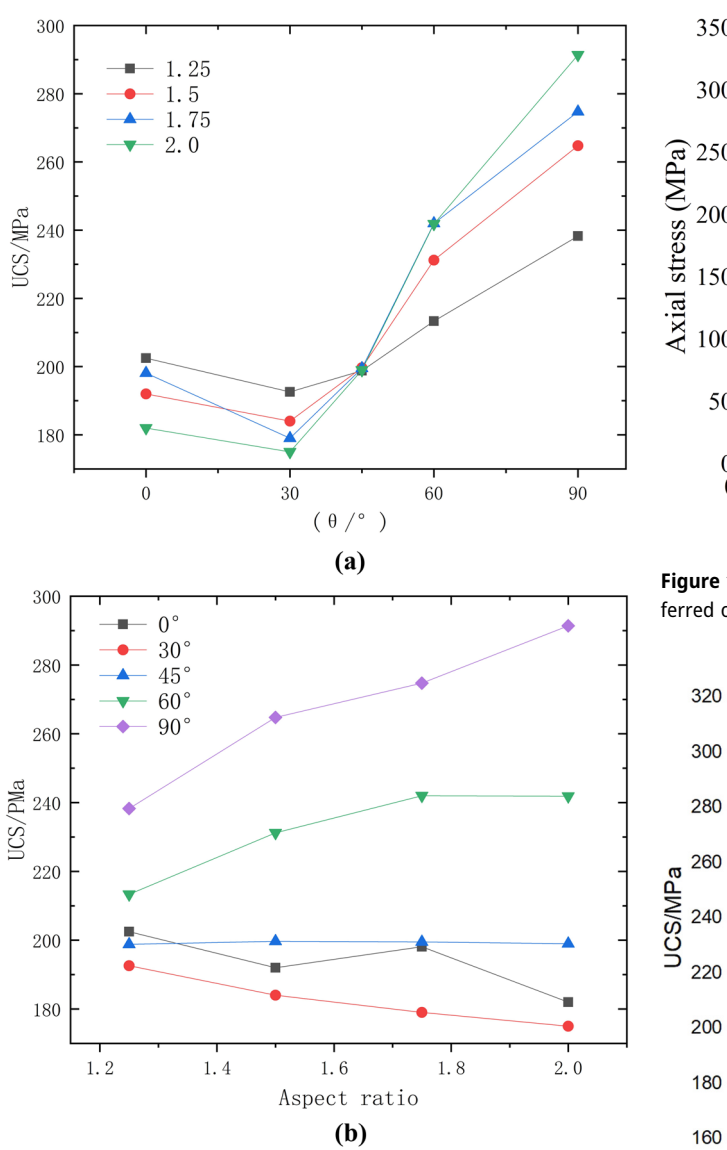


Figure 12: Relationship between UCS and rock grain with different aspect ratios and orientations: (a) different orientations and (b) different aspect ratios.

the curve occurred when the grain preferred orientation is around 30°. Moreover, when θ was between 0 and 30°, the UCS of the specimen decreased as the θ increased, and the UCS decreased as the grain aspect ratio increased. When θ was greater than 30°, the UCS of the specimen gradually increased and the larger the aspect ratio, the larger the UCS of the specimen at $\theta=90^\circ$. The angle corresponding to the inflection point of the curve was defined as the critical angle. When θ equals critical angle, the corresponding rock strength was the lowest. Thus, for the macroscopic mechanical properties of crystalline rocks with a preferred orientation, when the preferred orientation θ was less than the critical angle, the UCS of the rock decreased with the

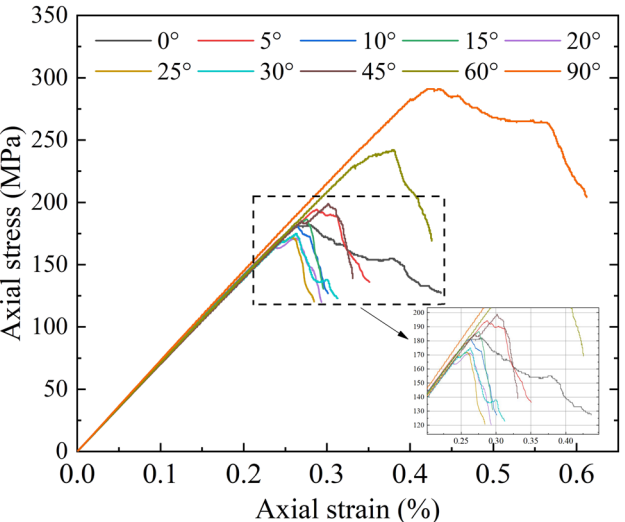


Figure 13: Stress–strain curve of rock samples with different grain preferred orientations.

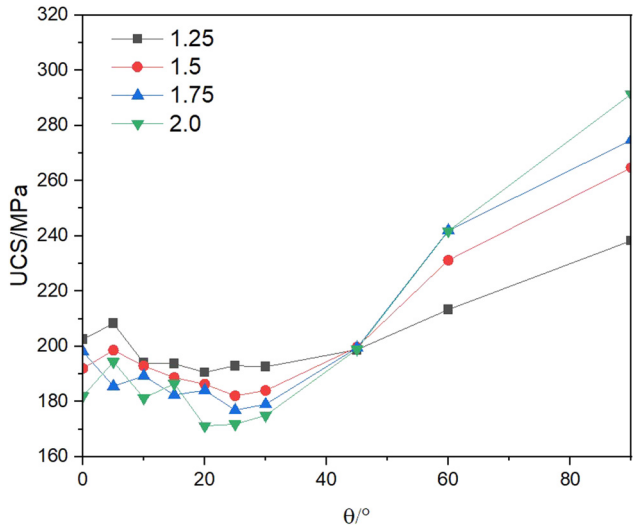


Figure 14: Variation of specimens' UCS (especially when θ was less than the critical angle).

increase of θ . Conversely, the UCS of rock was proportional to θ when θ was greater than the critical angle.

4.2 Features of fractures

4.2.1 Composition of fractures

The loading was stopped when the average stress of the wall (at the post-peak section of curve) reached 70% of the peak stress. It can be obtained that the change of crack evolution and macroscopic mechanical strength of the

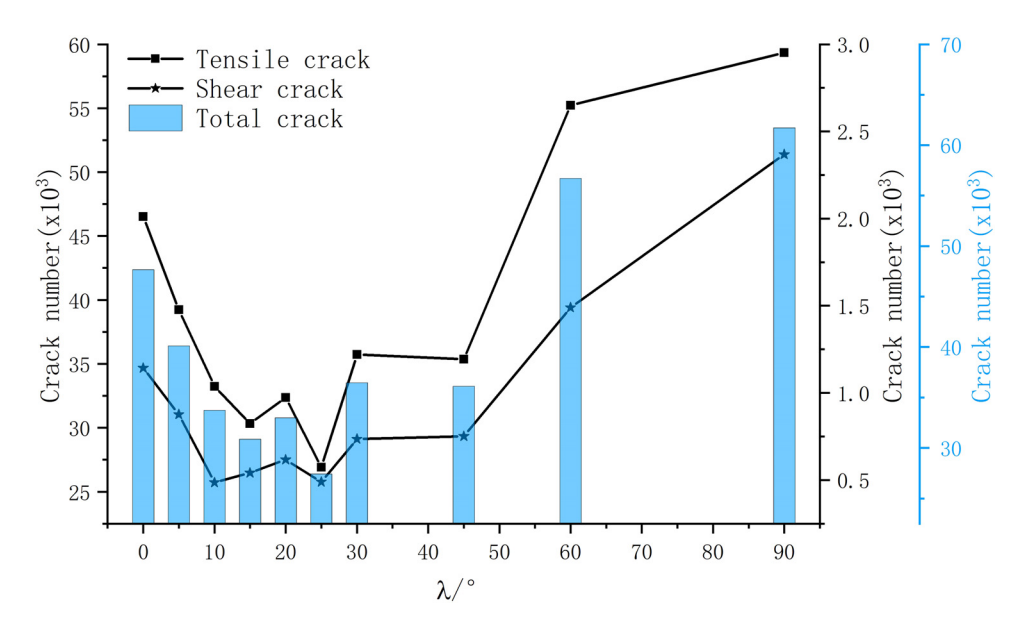


Figure 15: Effect of the preferred orientation of the grain on macroscopic cracks of rock specimens.

rock was similar under compression conditions. As λ got closer to the critical angle, the number of cracks decreased. The number of cracks (no matter shear cracks or tension cracks) reached a maximum when the loading angle was perpendicular to the preferred orientation of grain. In the PFC simulation model, the grain was made up of the ball groups and the contact between the balls. The actual resistance to external loads in the model was mainly a chain of forces consisting of contact. When the local tensile or shear stresses exceeded the limit strength of the contact, a fracture was generated at the position of the contact. Therefore, for models with a similar number of contacts, the more fractures were generated at the time of failure, the more the

contact resisted the external forces in the model. Therefore, it can be seen that there was an inversion point appeared in tensile and shear cracks curve when λ got closer to the critical angle and the load carrying capacity of the specimen was also lower at this point. However, the macroscopic mechanical strength of the material reached its maximum value (*e.g.*, λ = 90°), as shown in Figure 15.

Furthermore, in crystalline rocks, the minerals exhibit substantial mechanical strength, while the interfaces between these minerals display comparatively lower quality. The damage in such rocks initiates from the breakdown of intergranular weak surfaces, progressively advancing toward the crystal's interior. The rock's load-bearing capacity is

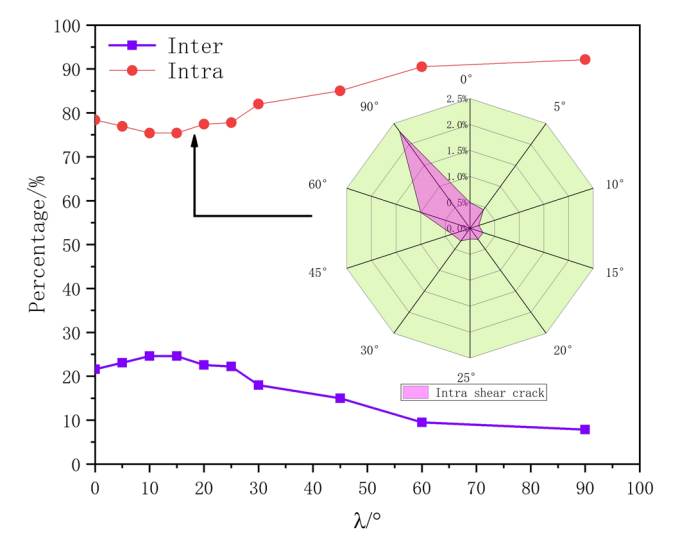


Figure 16: Effect of the preferred orientation on intracrystalline and intergranular cracks.

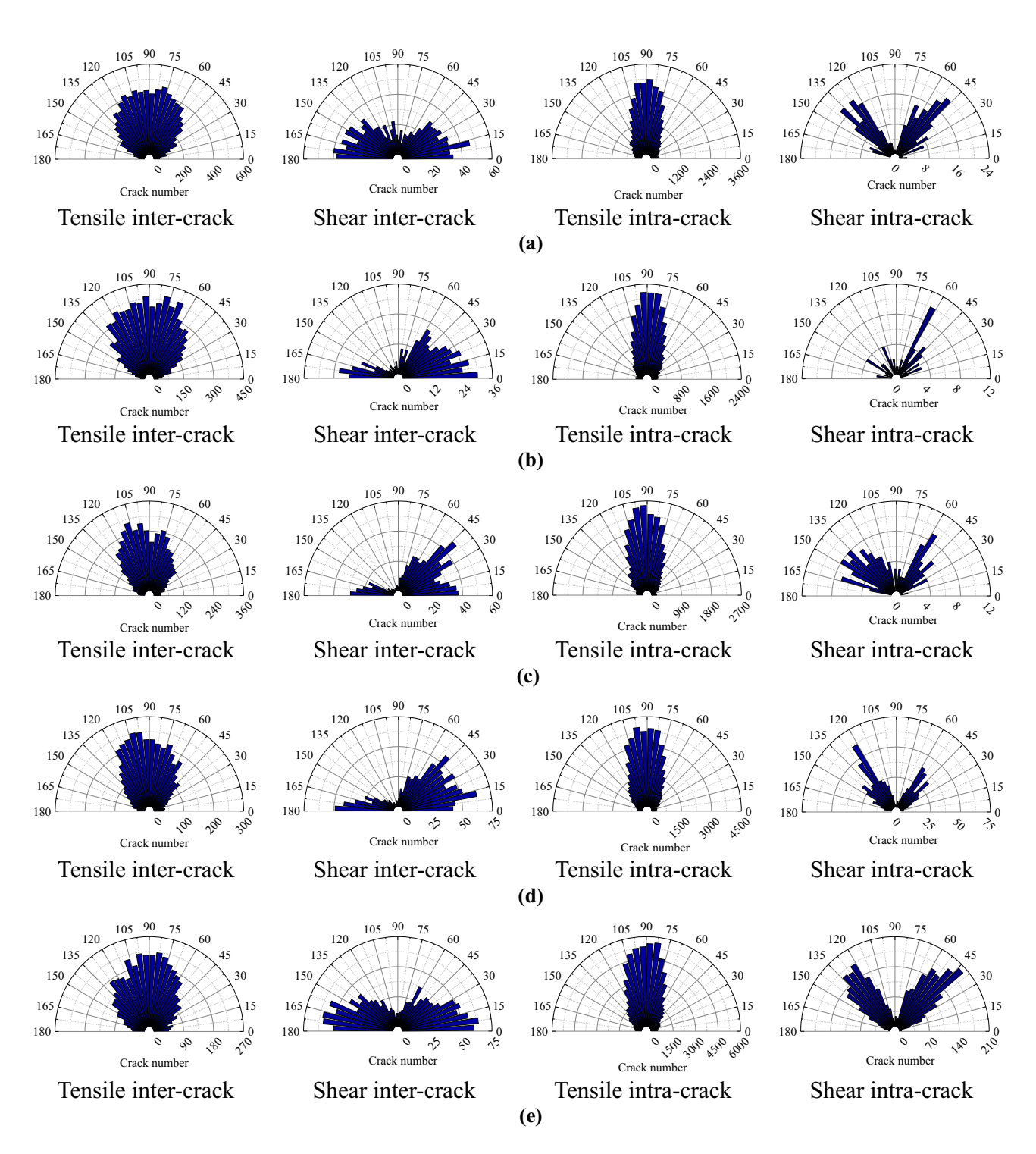


Figure 17: Microcrack orientation in the numerical models with different grain preferred orientations: (a) loading angle = 0°, (b) loading angle = 10°, (c) loading angle = 45° , (d) loading angle = 60° , and (e) loading angle = 90° .

compromised directly upon the formation of a penetration surface within the crystals. Alternatively, stress diffusion into the crystals induces intracrystalline damage that ultimately leads to the creation of a continuous surface. The escalation in intracrystalline cracking corresponds to a heightened

DE GRUYTER

proportional contribution of minerals (the primary bearers of the rock's load-bearing capacity) to the rock's resilience against damage. Thus, the presence of intracrystalline cracks can, to some extent, signify alterations in macroscopic strength. As shown in Figure 16, during compression, intracrystalline cracks account for a larger proportion compared to intergranular cracks and are the main crack type in the rock specimen. With the increase of λ , the overall trend of intergranular cracks was decreasing, while the intracrystalline cracks increased slowly, and the two were in a reciprocal trend. When λ was 90°, the percentage of intracrystalline cracks reached over 90%, and the load-bearing capacity of the material was fully exploited. This was also consistent with the macroscopic strength change of the rock. More notably, as λ increased, the proportion of intracrystalline shear cracks to the total shear cracks became larger. This suggested that the intracrystalline cracks in the model tend to produce local shear damage when λ became larger. Usually, the shear strength of the rock was much greater than the tensile strength, so this was one of the reasons for the increase in final macroscopic strength.

4.2.2 Direction of fractures

Under uniaxial compression conditions, the orientation of both intergranular and intragranular cracks was roughly parallel to the loading direction (*i.e.*, concentrated around 90°), which was more consistent with the existing research results. However, as λ increased from 0 to 90°, it can be found from the rose diagram that the crack orientation slowly expanded regardless of whether it was an intragrain tension crack or a shear crack. As shown in Figure 17, whichever direction has the largest percentage of cracks is defined as the dominant crack direction. It can be seen that this was just the opposite of the trend of UCS with λ (from 0° to 90°). The statistical analysis showed that the dominant crack orientation was roughly 45°, 65°, 55°, 55°, and 35° when λ is 0°, 10°, 45°, 60°, and 90°, respectively. This verified the

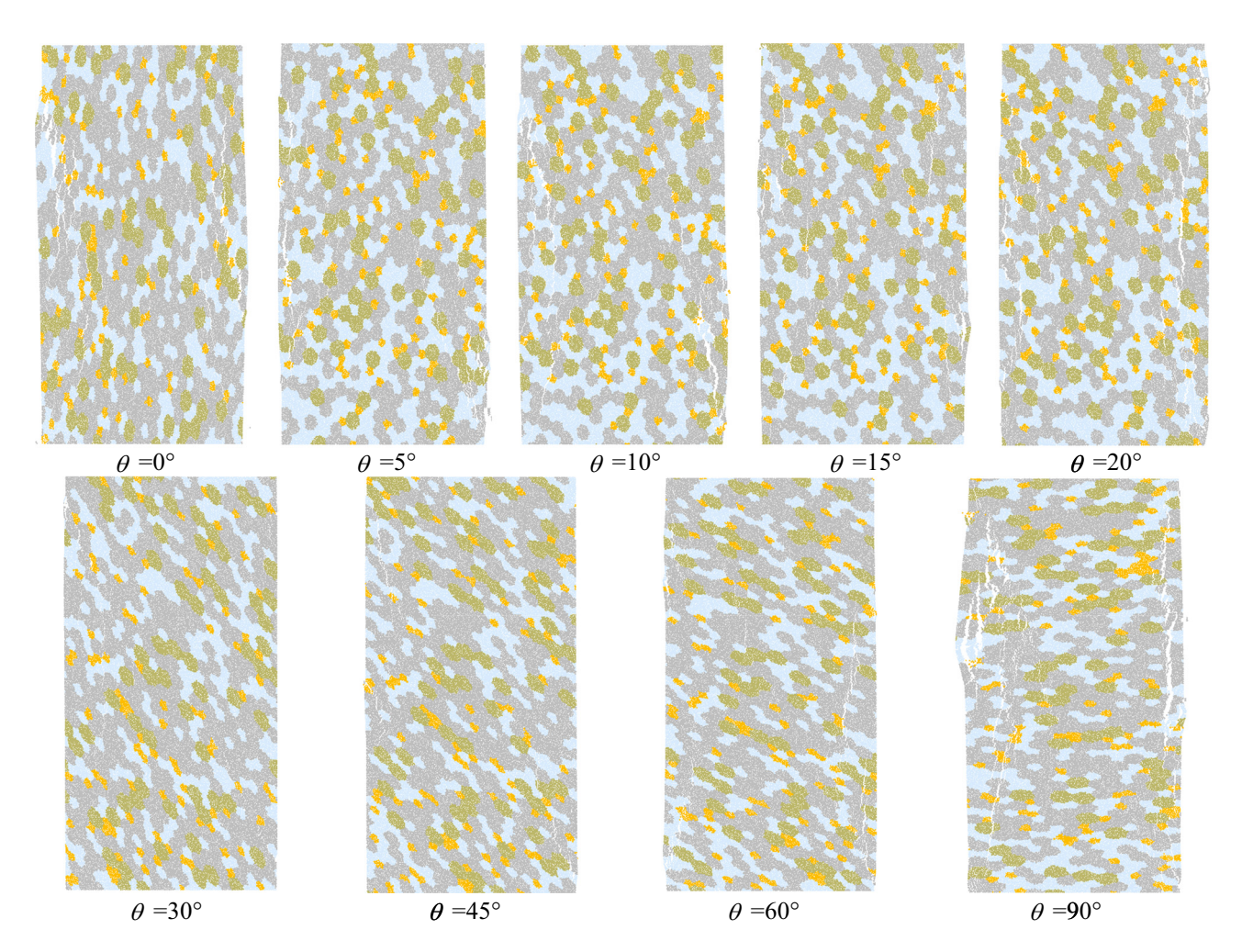


Figure 18: Effect of the preferred orientation on the macro failure characteristics.

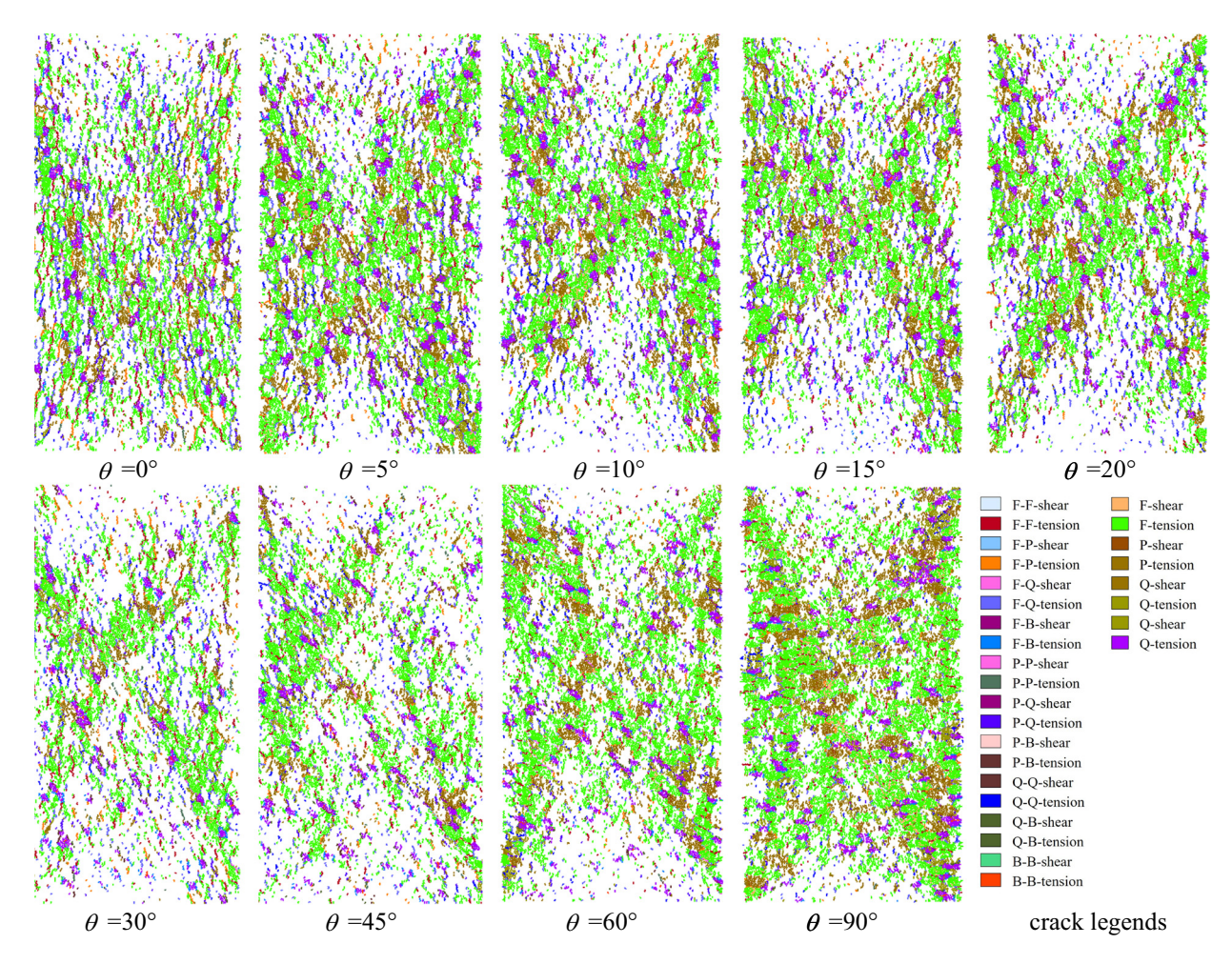


Figure 19: Effect of the preferred orientation on the microcrack distribution.

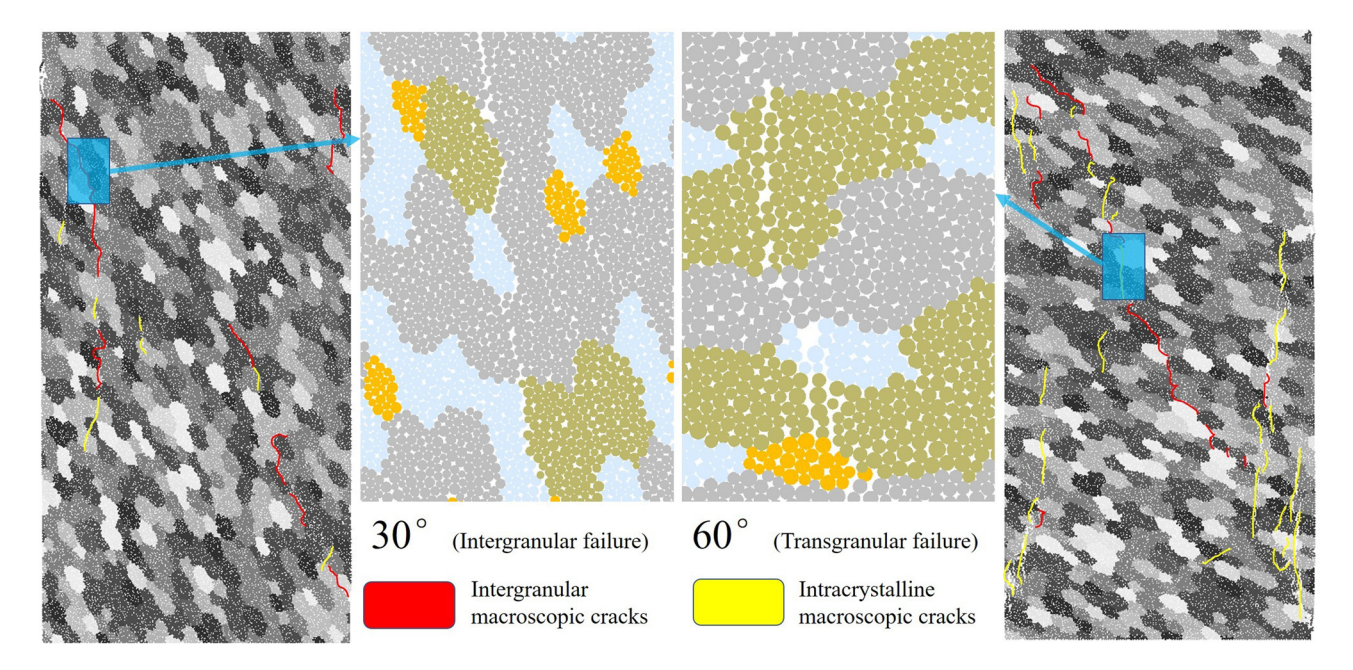


Figure 20: Micro-failure modes and damage features of crystalline rock under uniaxial compression.

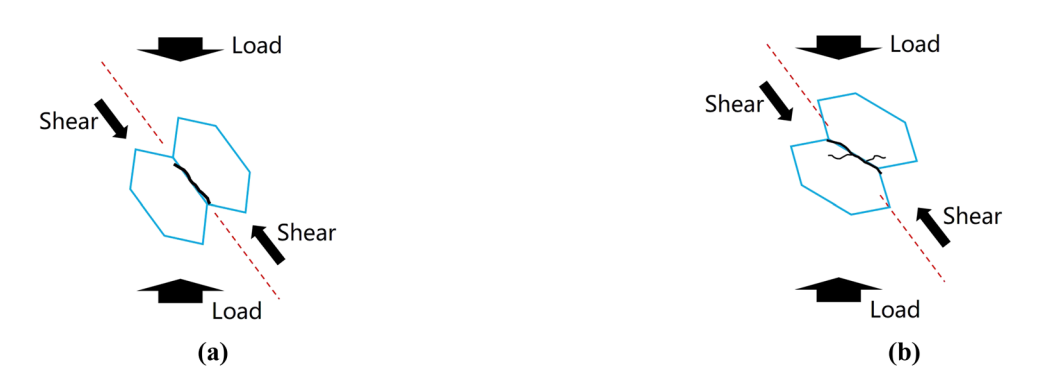


Figure 21: Mechanisms of grain destruction with different preferred orientations and loading directions: (a) θ is close to the stress damage direction and (b) θ deviates from the stress damage direction.

correlation between the macroscopic mechanical strength of the rock and the crack evolution obtained from the previous study. The intergranular tensile crack variation had a similar pattern. In fact, when the grain preferred orientation deviated from the final damage direction, cracks were generated within the crystal due to crystal extrusion, and this cracking due to extrusion was irregular and the direction of the cracking was more random.

4.3 Failure mode

The typical failure patterns of the samples with different preferred orientations are shown in Figure 18. It can be seen that the macroscopic failure mode of rock was presented as an axial splitting tensile failure. There were fewer macroscopic cracks when λ got closer to the critical angle while macroscopic cracks increased significantly when the difference between λ and θ became larger. Obvious fracture damage caused by axial pressure can be seen from the middle to both sides of the specimen. Especially when λ equals 90°, the vertical crack penetration was high, and there

was serious damage and a spalling trend at the side of the specimen. However, when the value of λ was from 5 to 20°, only a small amount of cracks were locally generated but not connected, reducing the integrity of the rock.

From the distribution of microcracks, it can be obtained from Figure 19 that fewer cracks developed in the specimen when λ was closer to 30°. As λ increased in the opposite direction (from 20° to 0°), the central cracks gradually increased and were eventually distributed near the fracture surface. When λ was more than 60°, the microcracks were distributed over a more extensive area and formed a clear "X" distribution pattern gradually [50]. Further observation on the crystal scale revealed that the damage pattern of the specimen varied with the preferred orientation of grains. Two types of damage modes occurred under uniaxial compression: intergranular failure and intragranular failure, and both were coexisting states. The intracrystalline failure was more observed for specimens with a preferred orientation of 0-20° and 60-90° while for the 30° and 45° cases the intergranular failures were more encountered. Taking λ = 30° and 60° as an example. It can be seen from Figure 20 that the number of penetration cracks and intergranular cracks

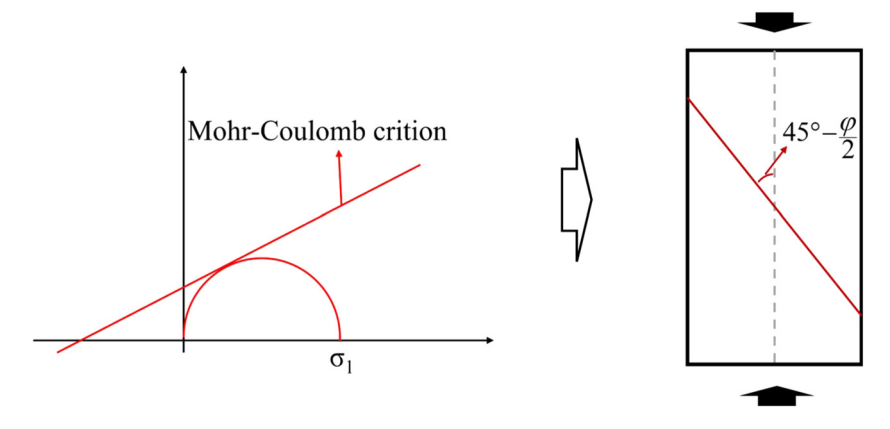


Figure 22: Schematic diagram of the fracture surface of the macroscopic rock mass.

increased significantly at $\lambda=60^\circ$, and the crack penetration length was longer. In addition, when $\lambda=30^\circ$, the penetration cracks were mostly distributed on both edges, but the penetration cracks also appeared in the middle part of the specimen at 60° .

5 Discussion

The article concentrated on the macro-mechanical response and micro-evolutionary mechanisms of crystalline rocks exhibiting varied grain orientations under axial loading. Utilizing the MTM, the embedded FISH language controls random mineral seed size and distribution patterns to create Tyson polygons. A polygonal geometry that matches the rock texture is obtained as a grain boundary by spatially transforming the vertices of the Tyson polygon. In comparison to similar research, this article presented two primary focal points: (1) Introducing a novel approach to establishing a GBM with specific aspect ratios and preferred orientations based on the conventional GBM utilizing Tyson polygons in PFC. (2) Analyzing, for the first time, the impact and mechanism of load direction and grain preferred orientation on the macroscopic mechanical properties, microscopic crack evolution, and damage mode of crystalline rocks across multiple scales.

The research results indicated that the GBM studied in this article can be divided into an intra-granular contact model (FJM) and an intergranular contact model (SJM). Usually, the intergranular contact surface is a "weak field surface" with relatively low strength. Therefore, intergranular cracks tend to

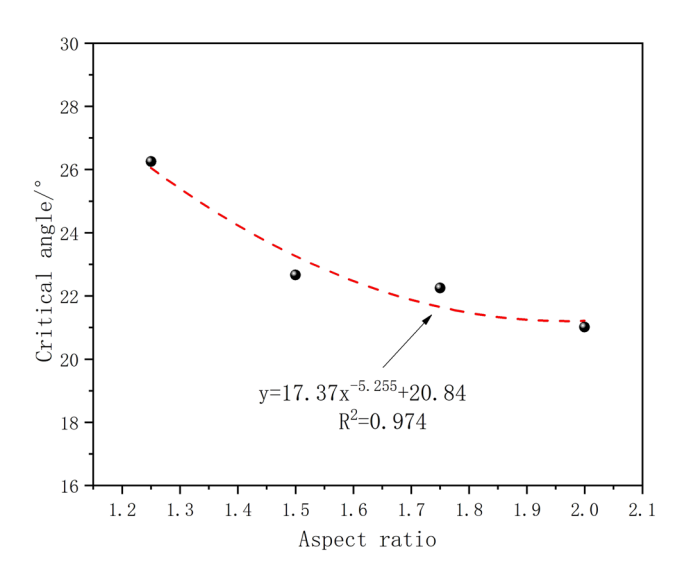


Figure 23: Effect of grain aspect ratio on the critical angle.

appear earlier in the stress transfer process [37]. In addition, the FIM model is based on the x- and y-coordinates of the global coordinate system, while the SJM model differs from the FJM model in that the mechanical calculations are updated based on the vertical and tangential directions of the joint (the edge corresponding to the Tyson polygon in GBM), which makes the ball-ball contact between two crystals more "smooth" [47]. Under external loading, shear stresses spread rapidly and are transmitted in the direction of cleavage damage. When the local shear force is greater than the shear strength of the SIM or FIM model, microcracks are formed. When the preferred orientation of grain is parallel to the dominant direction of the maximum shear stress in the model, the weak contact surfaces between the crystals are more likely to break under the misaligned shear of the crystals with greater stiffness on both sides, as in Figure 21(a). And when the preferred orientation of grain deviates from the direction of the maximum shear stress, the transfer of stress needs to overcome both the intergranular interface resistance and the intracrystalline material resistance. At this time, the normal extrusion force also aggravates the fracture of the contact, as shown in Figure 21(b). When the crack develops from intergranular to intracrystalline, more energy is needed to break the FJM contact that possesses greater roughness, which adds difficulties to the formation and penetration of macroscopic cracks in the model.

From the macroscopic mechanical properties of the rock, the initiation of cracking is due to the development and expansion of internal tension cracks, but its final damage is due to the through shear zone formed on the specimen. Elastic calculations based on the Moore–Coulomb theory can obtain the angle between the final shear damage zone of the rock and the main stress loading direction under uniaxial compression conditions as $(45-\varphi/2)$, as shown in Figure 22. The internal friction angle of crystalline rock is generally

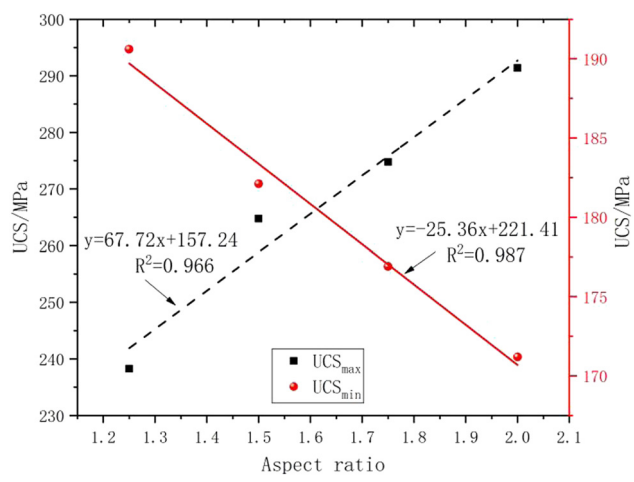


Figure 24: Effect of grain aspect ratio on UCS of rock.

40–50°, so the angle between the rupture surface and the main stress direction is roughly 20–25°. The compressive strength of the specimen reaches its lowest when the stress direction of the crystalline rock is closer to the crystal meritocratic orientation (the direction of the final rupture surface). Conversely, the mechanical strength of the rock is higher.

Although the critical angle obtained in the numerical tests is close to theoretical calculated values, there is still a deviation of within 5° (Figure 23). This is due to the fact that the numerical simulation of uniaxial compression was carried out mainly for rock samples with different preferred orientations of grain in this article, and the influence of the aspect ratio of grain on the microscopic frictional properties of crystalline rock grains was not considered much this time. In fact, the variation of mechanical strength of crystalline rock with loading angle for different grain aspect ratios can be found that as the aspect ratio varies between 1.25 and 2.0, the critical angle also varies in the range from 20° to 27°. The two factors are related by a quadratic function. The larger the aspect ratio is, the smaller the critical angle is, and the variation of the critical angle tends to flatten out at the aspect ratio of 2.0. Thus, based on the new modeling method proposed in this article, the grain aspect ratio parameter is set as a constant value of 2.0. Moreover, as shown in Figure 24, the grain aspect ratio is linearly related to the UCS of the rock specimen. The difference is that UCS_{max} is positively correlated with the aspect ratio, while UCS_{min} is negatively correlated with the aspect ratio. Therefore, for geotechnical engineering in actual crystalline rock formations, the relationship between the loading angle and preferred orientation, aspect ratio of grain has a large influence on the macroscopic mechanical properties of the rock [51]. This is also one of the key concerns when conducting simulation analysis and stability evaluation of rock properties in such formations. We will give more consideration to the effect of the aspect ratio in our subsequent study and how to extend the research methods and results to more complex 3D models with stress transfer and spatial structure.

6 Conclusion

This article introduces a novel GBM implemented by MTM in PFC^{2D}, capable of generating specified aspect ratios and crystallographic orientations. A standardized calibration process for the model parameters was outlined. Subsequently, utilizing the new model, the study investigated the impact of the angle between the primary stress direction of the crystalline rock and the model's grain-preferred orientation on the

fracture process and failure mode. This encompassed an analysis of the macroscopic mechanical properties, microscopic crack evolution, and the typical damage mode of the rock. Finally, the study delved into the destruction process and microscopic mechanisms of this particular type of crystalline rock under various loading angles, resulting in the following conclusions:

- 1) The novel GBM outlined in this article considers both the aspect ratio and crystal orientation. A program code was developed to extend and rotate the conventional Tyson polygon, assigning geometric orientation properties to the crystals. The numerical test results demonstrated the model's capability to investigate the mechanical response and microscopic characteristics of crystalline rocks exhibiting various grain-preferred orientations under diverse external loading directions.
- 2) The angle between the loading direction and crystal orientation significantly influenced the macroscopic mechanical properties of preferentially oriented crystalline rocks. Proximity to the critical angle resulted in diminished macro-mechanical strength of the rock. Conversely, a greater deviation from the critical angle led to increased macro-mechanical strength during the uniaxial compression process.
- 3) An inversion point occurred in the curve depicting tensile and shear cracks as the angle between the loading direction and preferred orientation approached the critical angle, resulting in a reduced load-carrying capacity of the specimen. The maximum number of cracks coincided with the loading angle being perpendicular to the preferred grain orientation, aligning with the material's peak macroscopic mechanical strength.
- 4) There were two coexisting damage modes of crystalline rocks under uniaxial compression: intergranular failure and intragranular failure. The damage pattern varied based on the preferred orientation of grains and the direction of external loading. A larger proportion of intergranular cracks occurred when the angle between the preferred orientation and loading direction was below the critical angle. At a 90° angle, crystal penetration failure became the primary form of rock damage, accompanied by a certain level of intergranular damage, fully utilizing the material's load-bearing capacity.

Funding information: This paper was supported by opening research project (KF2021-09), S&T Program of Hebei (225676162GH), China Postdoctoral Science Foundation (2023M744103) and Sichuan Science and Technology Program (grant number 2022NSFSC1176).

Author contributions: YP Hu: writing – original draft; ZR Zhang: writing - review and editing; ZW Yan: numerical simulation; YC Dong: writing - supervision and funding acquisition; YQ Zhu: conceptualization; ZR Xia: article framing; ZW Yan: editing; TD Guo: resources; WX Long: supervision. All authors have accepted responsibility for the entire content of this manuscript and approved its submission.

Conflict of interest: The authors state no conflict of interest.

References

- Blair, S. C. and N. Cook. Analysis of compressive fracture in rock using statistical techniques: Part II. Effect of microscale heterogeneity on macroscopic deformation. International Journal of Rock Mechanics and Mining Sciences, Vol. 35, No. 7, 1998, pp. 849–861.
- Zhou, L. J., S. L. Xu, J. F. Shan, Y. Liu, and P. Wang. Heterogeneity in deformation of granite under dynamic combined compression/ shear loading. Mechanics of Materials, Vol. 123, 2018, pp. 1–18.
- Pan, C., X. Li, L. He, and J. Li. Study on the effect of micro-geometric heterogeneity on mechanical properties of brittle rock using a grain-based discrete element method coupling with the cohesive zone model. International Journal of Rock Mechanics and Mining Sciences, 2021, id. 140.
- Xiao, H. G., L. He, X. Li, Q. Zhang, and W. Li. Texture synthesis: A novel method for generating digital models with heterogeneous diversity of rock materials and its CGM verification. Computers and Geotechnics, Vol. 130, 2021, id. 103895.
- Liu, G., M. Cai, and M. Huang. Mechanical properties of brittle rock governed by micro-geometric heterogeneity. Computers and Geotechnics, Vol. 104, 2018, pp. 358-372.
- Hemmati, A., M. Ghafoori, H. Moomivand, and G. R. Lashkaripour. The effect of mineralogy and textural characteristics on the strength of crystalline igneous rocks using image-based textural quantification. Engineering Geology, Vol. 266, 2020, id. 105467.
- Zhang, S., S. Qiu, P. Kou, S. Li, P. Li, and S. Yan. Investigation of damage evolution in heterogeneous rock based on the grain-based finite-discrete element model. Materials, Vol. 14, No. 14, 2021, pp. 39-69.
- [8] Zhang, S., S. Qiu, P. Li, Y. Kou, Z. Xie, and L. Jia. Mode I fracture behavior of heterogeneous granite: Insights from grain-based FDEM modelling. Engineering Fracture Mechanics, 2023, id. 284.
- Tang, C. A., L. G., Tham, P. Lee, Y. Tsui, and L. Tham. Numerical studies of the influence of microstructure on rock failure in uniaxial compression - Part II: Constraint, slenderness and size effect. International Journal of Rock Mechanics and Mining Sciences, Vol. 37, No. 4, 2000, pp. 571-583.
- [10] Gallagher Jr, J. J., M. Friedman, J. Handin, and G. M. Sowers. Experimental studies relating to microfracture in sandstone. Tectonophysics, Vol. 21, No. 3, 1974.
- [11] Irfan, T. Y. Mineralogy, fabric properties and classification of weathered granites in Hong Kong. Quarterly Journal of Engineering Geology and Hydrogeology, Vol. 29, 1996, pp. 5-35.
- [12] Eberhardt, E., B. Stimpson, and D. Stead. Effects of grain size on the initiation and propagation thresholds of stress-induced brittle

- fractures. Rock Mechanics and Rock Engineering, Vol. 32, No. 2, 1999, pp. 81-99.
- [13] Fujii, Y., T. Takemura, M. Takahashi, and W. Lin. Surface features of uniaxial tensile fractures and their relation to rock anisotropy in Inada granite. International Journal of Rock Mechanics and Mining Sciences, Vol. 44, No. 1, 2007, pp. 98-107.
- Undul, O. Assessment of mineralogical and petrographic factors affecting petro-physical properties, strength and cracking processes of volcanic rocks. Engineering Geology, Vol. 210, 2016, pp. 10-22.
- [15] Undul, O., F. Amann, N. Aysal, and M. L. Plötze. Micro-textural effects on crack initiation and crack propagation of andesitic rocks. Engineering Geology, Vol. 193, 2015, pp. 267-275.
- [16] Tugrul, A. and I. H. Zarif, Correlation of mineralogical and textural characteristics with engineering properties of selected granitic rocks from Turkey. Engineering Geology, Vol. 51, No. 4, 1999, pp. 303-317.
- [17] Hallbauer, D. K., H. Wagner, and N. G. W. Cook. Some observations concerning the microscopic and mechanical behaviour of quartzite specimens in stiff, triaxial compression tests. International Journal of Rock Mechanics and Mining Sciences & Geomechanics Abstracts, Vol. 10, No. 6, 1973, pp. 713-726.
- Prikryl, R. Some microstructural aspects of strength variation in rocks. International Journal of Rock Mechanics and Mining Sciences, Vol. 38, No. 5, 2001, pp. 671-682.
- Atapour, H. and A. Mortazavi. The influence of mean grain size on unconfined compressive strength of weakly consolidated reservoir sandstones. Journal of Petroleum Science and Engineering, Vol. 171, 2018, pp. 63-70.
- [20] Zheng, W. B. and D. D. Tannant. Grain breakage criteria for discrete element models of sand crushing under one-dimensional compression. Computers and Geotechnics, Vol. 95, 2018, pp. 231-239.
- Feng, Q., S. Hou, W. Liu, S. Zhang, W. Li, and M. Tian. Study on the simulation method and mesoscopic characteristics of rock freezethaw damage. Computers and Geotechnics, Vol. 153, 2023, id. 105038.
- [22] Cundall, P. A. A computer model for simulating progressive large scale movements in blocky rock systems[C]. In Proceedings of the Symposium of the International Society of Rock Mechanics (Nancy, France, 1971), Vol. 1, 1971, Paper No. II-8.
- [23] Bahrani, N. and P. K. Kaiser. Numerical investigation of the influence of specimen size on the unconfined strength of defected rocks. Computers and Geotechnics, Vol. 77, 2016, pp. 56-67.
- [24] Huang, Y. H., S. Q. Yang, P. G. Ranjith, and J. Zhao. Strength failure behavior and crack evolution mechanism of granite containing preexisting non-coplanar holes: Experimental study and particle flow modeling. Computers and Geotechnics, Vol. 88, 2017, pp. 182-198.
- [25] Yin, T. B., D. D. Zhuang, M. J. Li, and X. B. Li. Numerical simulation study on the thermal stress evolution and thermal cracking law of granite under heat conduction. Computers and Geotechnics, Vol. 148, 2022, id. 104813.
- [26] Wong, L., J. Peng, and C. I. Teh. Numerical investigation of mineralogical composition effect on strength and micro-cracking behavior of crystalline rocks. Journal of Natural Gas Science and Engineering, Vol. 53, 2018, pp. 191-203.
- Gao, F. Q. and H. P. Kang. Grain-based discrete-element modeling study on the effects of cementation on the mechanical behavior of low-porosity brittle rocks. *International Journal of Geomechanics*, Vol. 17, No. 9, 2017

- [28] Sinha, S. and G. Walton. A study on Bonded Block Model (BBM) complexity for simulation of laboratory-scale stress-strain behavior in granitic rocks. *Computers and Geotechnics*, Vol. 118, 2020, id. 103363.
- [29] Li, X. F., Q. B. Zhang, H. B. Li, and J. Zhao. Grain-based discrete element method (GB-DEM) modelling of multi-scale fracturing in rocks under dynamic loading. *Rock Mechanics and Rock Engineering*, Vol. 51, No. 12, 2018, pp. 3785–3817.
- [30] Ghazvinian, E., M. S, Diederichs, and R. Quey. 3D random Voronoi grain-based models for simulation of brittle rock damage and fabric-guided micro-fracturing. *Journal of Rock Mechanics and Geotechnical Engineering*, Vol. 6, No. 6, 2014, pp. 506–521.
- [31] De Silva, V. R. S., H. Konietzky, H. Märten, P. G. Ranjith, Z. Lei, and T. Xu. Grain-scale numerical simulation of crystalline rock fracturing using soundless cracking demolition agents for in-situ preconditioning. *Computers and Geotechnics*, Vol. 155, 2023, id. 105187.
- [32] Potyondy, D. O. A grain-based model for rock: Approaching The True Microstructure. *In Proceedings of rock mechanics in the Nordic Countries*, 2010, pp. 9–12.
- [33] Potyondy, D. O. A flat-jointed bonded-particle model for rock. Paper presented at the 52nd U.SRock Mechanics/Geomechanics Symposium, Seattle, Washington, June 2018.
- [34] Potyondy, D. O. A flat-jointed bonded-particle material for hard rock. Paper presented at the 46th U.SRock Mechanics/Geomechanics Symposium, Chicago, Illinois, June 2012.
- [35] Potyondy, D. "PFC3D Flat-Joint Contact Model (version 1)," Itasca Consulting Group, Inc., Minneapolis, MN, Technical Memorandum ICG7234-L, June 25, 2013.
- [36] Potyondy, D. "PFC2D Flat-Joint Contact Model," Itasca Consulting Group, Inc., Minneapolis, MN, Technical Memorandum ICG7138-L, July 26, 2012.
- [37] Zhou, J., H. Lan, L. Zhang, D. Yang, J. Song, and S. Wang. Novel grain-based model for simulation of brittle failure of Alxa porphyritic granite. *Engineering Geology*, Vol. 251, 2019, pp. 100–114.
- [38] Peng, J., L. N. Wong, C. I. Teh, and Z. Li. Modeling micro-cracking behavior of bukit timah granite using grain-based model. *Rock Mechanics and Rock Engineering*, Vol. 51, No. 1, 2018, pp. 135–154.
- [39] Peng, K., Y. Zhang, X. Xu, J. Han, and Y. Luo. Numerical investigation of brittleness effect on strength and microcracking behavior of crystalline rock. *International Journal of Geomechanics*, Vol. 22, No. 10, 2022, id. 04022178.
- [40] Eberhardt, E., D. Stead, B. Stimpson, and R. S. Read. Identifying crack initiation and propagation thresholds in brittle rock. *Canadian Geotechnical Journal*, Vol. 35, No. 2, 1998, pp. 222–233.

- [41] Diederichs, M. S., P. K. Kaiser, and E. Eberhardt. Damage initiation and propagation in hard rock during tunnelling and the influence of near-face stress rotation. *International Journal of Rock Mechanics* and Mining Sciences, Vol. 41, No. 5, 2004, pp. 785–812.
- [42] Wong, L., and H. H. Einstein. Crack coalescence in molded gypsum and carrara marble: Part 1. macroscopic observations and interpretation. *Rock Mechanics and Rock Engineering*, Vol. 42, No. 3, 2009, pp. 475–511.
- [43] Bahrani, N., P. K. Kaiser, and B. Valley. Distinct element method simulation of an analogue for a highly interlocked, non-persistently jointed rockmass. *International Journal of Rock Mechanics and Mining Sciences*, Vol. 71, 2014, pp. 117–130.
- [44] Wong, L., and Y. H. Zhang. An extended grain-based model for characterizing crystalline materials: An example of Marble. Advanced Theory and Simulations, Vol. 1, No. 8, 2018, id. 1800039.
- [45] Zhao, X., D. Elsworth, Y. He, W. Hu, and T. Wang. A grain texture model to investigate effects of grain shape and orientation on macro-mechanical behavior of crystalline rock. *International Journal of Rock Mechanics and Mining Sciences*, Vol. 148, 2021, id. 104971.
- [46] Zhang, T., L. Yu, Y. Peng, H. Jing, H. Su, and J. Wei. Effect of the mineral spatial distribution heterogeneity on the tensile strength of granite: Insights from PFC3D-GBM numerical analysis. *Journal of Rock Mechanics and Geotechnical Engineering*, Vol.15, 2022, pp. 1144–1160.
- [47] Mehranpour, M. H. and P. H. Kulatilake. Improvements for the smooth joint contact model of the particle flow code and its applications. *Computers and Geotechnics*, Vol. 87, 2017, pp. 163–177.
- [48] Wu, S. and X. Xu. A study of three intrinsic problems of the classic discrete element method using flat-joint model. *Rock Mechanics and Rock Engineering*, Vol. 49, 2016, pp. 1813–1830.
- [49] Hofmann, H., T. Babadagli, J. S. Yoon, A. Zang, and G. Zimmermann. A grain based modeling study of mineralogical factors affecting strength, elastic behavior and micro fracture development during compression tests in granites. *Engineering Fracture Mechanics*, Vol. 147, 2015, pp. 261–275.
- [50] Nicksiar, M. and D. C. Martin. Factors affecting crack initiation in low porosity crystalline rocks. *Rock Mechanics and Rock Engineering*, Vol. 47, No. 4, 2014, pp. 1165–1181.
- [51] Menegon, L., G. Pennacchioni, R. Heilbronner, and L. Pittarello. Evolution of quartz microstructure and c-axis crystallographic preferred orientation within ductilely deformed granitoids (Arolla unit, Western Alps). *Journal of Structural Geology*, Vol. 30, No. 11, 2008, pp. 1332–1347.